Available online at www.sciencedirect.com
ScienceDirect
Geochimica et Cosmochimica Acta 71 (2007) 3476–3497
Geochimica et Cosmochimica Acta
www.elsevier.com/locate/gca

Geochemistry and morphology of metalliferous sediments and oxyhydroxides from the Endeavour segment, Juan de Fuca Ridge

Elitsa Hrischeva *, Steven D. Scott

Scotiabank Marine Geology Research Laboratory, Department of Geology, University of Toronto, Toronto, Ont., Canada M5S 3B1

Received 24 May 2006; accepted in revised form 5 March 2007; available online 4 April 2007

Abstract

We present first data on the geochemistry, mineralogy and morphology of near-vent sediments (35 and 200 m from active vent) and ridge flank sediments (approximately 3 km from the vent field) as well as oxyhydroxide deposits from the Endeavour segment, Juan de Fuca Ridge. The purpose of the study was to understand better the origin and characteristic features of metalliferous sediments associated with base and precious metal massive sulfides in volcanic terrains. Hydrothermal components in sediments are Fe–Si ± S-rich and Mn–Fe–Si-rich phases, sulfides and barite, which were exclusively derived from plume fallout. Sulfides are only a minor constituent of near-vent sediments (2–4 wt%) and were not detected in ridge flank sediments. The study suggests that the distribution of hydrothermal phases and associated elements in near-vent and ridge flank sediments is affected mainly by processes of agglomeration, dissolution, absorption and settling that take place within a plume and to a lesser extent post-depositional processes. Rapid deposition of sulfides in the vicinity of the vents is reflected in a sharp drop of the Cu concentrations in sediments with increasing distance from the vents. Besides sulfides, important carriers of Pb, Cu, Zn and Co in near-vent sediments are Fe–Mn oxyhydroxides that occur together with silica as aggregates of gel-like material and flaky particles and as coatings on filaments. Away from the vents, trace metals are mostly in Fe–Mn oxyhydroxides and authigenic Fe-rich montmorillonite. Oxyhydroxides at the Main Endeavour field are interpreted to have originated from oxidation of mound sulfides accompanied by precipitation of primary Fe-oxyhydroxide + silica from low-temperature fluids. At the Mothra field, seafloor deposits and chimney crusts composed of Fe-oxyhydroxide ± Mn + silica are considered to be direct precipitates from hydrothermal fluids that have been less diluted with seawater. Oxyhydroxide deposits exhibit unique microtextures that resemble mineralized microorganisms and may indicate existence of diverse microbial communities.

1. INTRODUCTION

Modern seafloor hydrothermal systems commonly have associated metalliferous sediments and Fe–Si–Mn oxyhydroxide deposits. Metalliferous sediments form mainly by dispersion of erosion products of chimneys and other hydrothermal precipitates and by fallout of particles from a hydrothermal plume (Mills, 1995 and references therein). Plumes containing sulfide, sulfate and oxyhydroxide particles rise tens to hundreds of meters in a vertically ascending buoyant mass and then spread laterally as a neutrally buoyant plume (Lupton et al., 1985; Baker and Massoth, 1987; McConachy and Scott, 1987). Numerical models of deposition and studies of the settling flux of hydrothermal plume particles have shown that the majority of large-grained black smoker particles should be deposited within a few hundred meters of the vent, while fine-grained particles, constituting more than 90 percent of the total particulate population, are transported beyond the ridge crest (Feely et al., 1987, 1992; Dymond and Roth, 1988). "Fallout" sediments, thus, can provide a record of the dispersal patterns and processes taking place within the plumes. The composition of sediments is further modified by post-depositional reactions such as oxidation/dissolution and scavenging (Ruhlin and Owen, 1986; Feely et al., 1987; German et al., 1997).

Iron-rich oxyhydroxide deposits occur in areas of high-temperature hydrothermal venting and deposition of

* Corresponding author. Fax: +1 416 978 3938.
E-mail address: hrischeva@geology.utoronto.ca (E. Hrischeva).

0016-7037/$ - see front matter © 2007 Elsevier Ltd. All rights reserved.
doi:10.1016/j.gca.2007.03.024

sulfides or are isolated from sulfides. Those spatially associated with sulfide deposits could be a product of sulfide oxidation, such as gossans on the TAG mound on the Mid-Atlantic Ridge (Hannington et al., 1988; Herzig et al., 1991; Mills and Elderfield, 1995) and the East Pacific Rise at 21°N and 12°N (Haymon and Kastner, 1981; Hekinian et al., 1993) or are primary precipitates from hydrothermal fluids, such as ochres and chimney oxides at TAG (Mills and Elderfield, 1995) and Fe-oxyhydroxides on the East Pacific Rise at 12°N (Hekinian et al., 1993). Iron- and silica-rich oxyhydroxide deposits isolated from sulfides are directly precipitated from low-temperature hydrothermal fluids (e.g., Puteanus et al., 1991; Binns et al., 1993; Hekinian et al., 1993; Boyd and Scott, 1999; Kennedy et al., 2003; Benjamin and Haymon, 2006).

Many ancient volcanogenic massive sulfide (VMS) deposits are overlain and flanked by ferruginous cherty sediments such as those in Kuroko deposits of Japan (Kalogeropoulos and Scott, 1983), the Noranda deposits of Quebec, Canada (Kalogeropoulos and Scott, 1989), and the Bathurst deposits in New Brunswick, Canada (Peter and Goodfellow, 1996; Peter et al., 2003). The rocks are thought to represent sediments that were deposited from hydrothermal fluids that vented at the seafloor and may be ancient analogues of the modern metalliferous sediments and oxyhydroxides in areas of volcanic activity. Many attempts to use the distribution of trace elements in such rocks as an exploration guide to VMS ores has been frustrated by inconsistent results. We have turned to active systems in an attempt to better understanding how trace elements, and particularly metals, are incorporated into metalliferous sediments.

In this paper, we present first data on the geochemistry, mineralogy and morphology of metalliferous sediments and oxyhydroxide deposits from the Endeavour segment, Juan de Fuca Ridge. The purpose of the study was to understand better how metalliferous deposits form around modern and, by analogy, ancient base and precious metal massive sulfides in volcanic terrains and to establish the geochemical and mineralogical signatures of hydrothermal materials of various origins. We also show images of unique microtextures that could be of microbial origin and may be of interest in studies on the biodiversity of the Endeavour segment.

2. GEOLOGICAL SETTING

The Endeavour segment comprises the northernmost portion of the intermediate spreading rate (30 mm/yr) Juan de Fuca Ridge (Fig. 1a). The segment, which is ~90 km in length, is bounded north and south by overlapping spreading centers (Karsten et al., 1986). The actively spreading portion of the Endeavour segment is flanked east and west by ridges and basins elongated parallel to the overall N20°E trend of the Juan de Fuca Ridge. The axial valley is well defined by a narrow zone of continuous fault scarps and fissuring (Tivey and Johnson, 1987). Direct observations from a submersible have shown that overlapping pillow, lobate and sheet flows have built the outer flanks of the central volcanic ridge of the Endeavour segment, while the fractured basaltic substrate of the main vent area is primarily composed of weathered pillow and lobate flows with ponded sediment (Tivey and Delaney, 1986; Delaney et al., 1992). The Endeavour segment is considered to be dominantly in an extensional tectonic phase, which sustains the hydrothermal activity throughout the central portion of the segment (Delaney et al., 1992). The hydrothermal activity is controlled by normal faults along the western valley wall of the segment (Tivey and Delaney, 1985).

Five major vent fields have been discovered along the Endeavour segment. From north to south the fields are Sasquatch, Salty Dawg, High Rise, Main Endeavour, and Mothra (Kelley et al., 2001a). The spacing between the distinct fields increases from north to south, which is accompanied by dramatic changes in the style, intensity and thermal-chemical characteristics of venting (Kelley et al., 2001a). The Main Endeavour field is located at 47°57′N and 129°06′W on the central and shoalest portion of the Endeavour segment at a depth of ~2200 m (Fig. 1b). It extends at least 350 m along the valley wall, is nearly 180 m wide and contains at least 15 large actively venting sulfide edifices and tens of smaller sulfide structures (Delaney et al., 1992). The Main Endeavour field is the most vigorously venting of the Endeavour vent fields, with high-temperature fluids of 345–400 °C (Delaney et al., 1984; Butterfield et al., 1994). Diffuse flow is also common both within and distal to the field (Kelley et al., 2001a). Within the vent field, low-temperature fluids exit from sulfide structures and basalts (Tivey and Delaney, 1986; Delaney et al., 1992). The Mothra vent field is at least ~500 m long and is the largest venting site of the Endeavour segment. There are at least five complexes of active and inactive sulfide pinnacles (Kelley et al., 2001b). In contrast to the Main Endeavour field, black smoker chimneys are rare in Mothra. Most of the sulfide structures are awash in diffusely venting fluids (30–200 °C) that support diverse macrofaunal and microbial communities (Kelley et al., 2001b; Kristall et al., 2006).

The high-temperature venting at the Endeavour segment results in buoyant plumes (Feely et al., 1987; Rona et al., 2002) and a large neutrally buoyant plume with a core depth of approximately 2000 m (Baker and Massoth, 1987; Feely et al., 1992; Thomson et al., 1992). The hydrothermal plume is characterized by high concentrations of particulate Cu, Fe, P, and As and has been traced at least 85 km to the west-southwest from the Endeavour vent field (Feely et al., 1992). The hydrothermal plumes rising from the vent fields drive a steady near-bottom inflow within the valley (Thomson et al., 2003).

3. SAMPLING AND METHODS

Samples for this study were collected by the ROPOS remotely operated vehicle during two expeditions to the Endeavour segment of the Juan de Fuca Ridge in 2003 and 2004. The sampling of sediments and other hydrothermal deposits were carried out along with microbiological experiments and deployment of various instruments on the seafloor, which are part of the Ridge 2000 Integrated Studies program. The samples taken for our study were opportunistic and do not cover a large part of the segment. Near-vent sediments accumulated in sediment ponds and

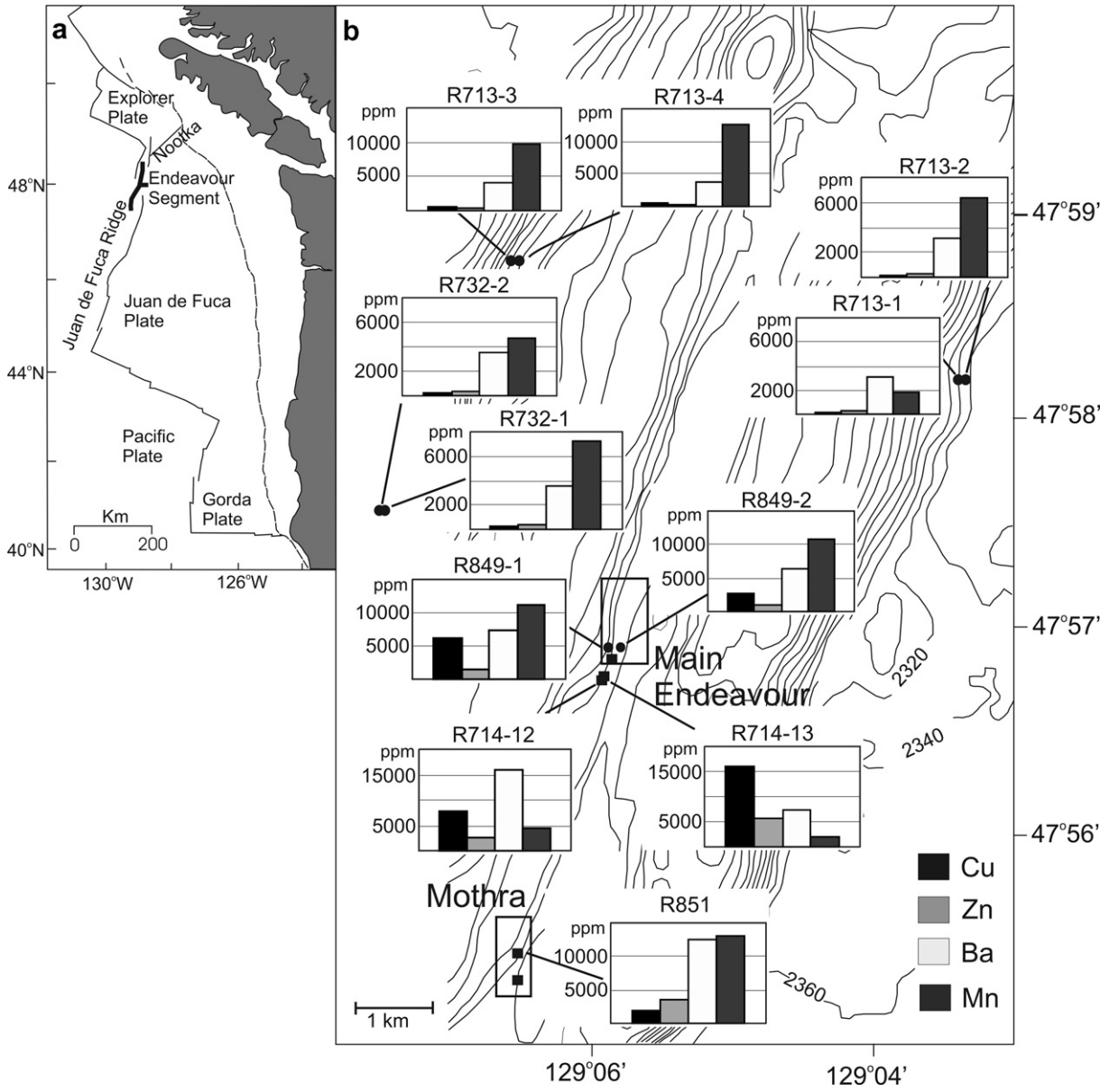

Fig. 1. (a) Location of the Endeavour segment along the Juan de Fuca Ridge. (b) Map of the Endeavour segment. Shown are the locations of the samples (circles—sediments; squares—oxyhydroxide deposits) and the distribution of the concentrations of Cu, Zn, Ba and Mn.

on basalt surfaces were taken by suction sampler 35 and 200 m from an actively venting structure, Grotto, located in the central portion of the Main Endeavor field. Ridge flank sediments were taken within approximately 3 km east and west of the ridge axis. Push core sampling was carried out where sediments were sufficiently thick and retrieved 20 cm of material. Suction samples were taken at places with thin sediment cover at the ridge flanks. Powdery orange to red oxyhydroxide deposits occurring as ponds in oxidized sulfides from a large old sulfide mound in the southern portion of the Main Endeavour field were sampled by push core sampler. In proximity to the oxyhydroxide deposits, eroded sulfide sediment was collected from the foot of a 15 m scarp below a sulfide structure. A suction sample recovering a 1 cm surface layer of a seafloor oxyhydroxide deposit as well as a fragment of an old extinct chimney were collected from the Mothra vent field. Hemipelagic sediments were sampled from a mud volcano with undefined hydrothermal activity at Nootka fault, which borders the Endeavour segment to the north (Fig. 1a).

Prior to analysis, samples were washed with distilled water to remove salts, dried at 80 °C and ground. The majority of the analytical work was conducted at the University of Toronto. Trace elements were analyzed by Instrumental Neutron Activation Analysis (INAA). Approximately 200 mg of sediment powder from each sub-sample was sealed into Sb-free doubly lined polyethylene bags following the procedure of Barnes and Gorton (1984). Seven days and 40 days after irradiation, sample counts were performed for various trace elements (Fe, Cr,

As, Co, Ni, Mo, Zn, Ba, Au, REE and U) using intrinsic Ge detectors. The accuracy of the INAA analyses determined using a basalt standard, UTB-1 (Stix and Gorton, 1992), was within 10% for Zn, Sm and Cr and within 5% for the rest of the elements. Analytical precisions were better than 5% for all elements except Cr (<10%). Concentrations of major elements as well as trace elements Cu, Zn, Pb, and Ba were determined by X-ray fluorescence (XRF). Selective leaching of two sediment samples was performed by ACTLABS of Burlington, Ontario. Samples were treated with hot hydroxylamine leach for dissolution of Mn and Fe-oxyhydroxides and concentrations of Fe, Mn, Cr, Co, Ni, Cu, Zn, and Pb in the leachate were analyzed by atomic absorption spectroscopy (AAS).

Mineralogical study of sediments and oxyhydroxides was conducted by X-ray powder diffraction on a Philips diffractometer using CuK_{α} radiation operating at 40 kV and 40 mA, at a scan rate of 1° per minute. Bulk samples and sediment clay fractions <4, <2 and <0.2 μm were separated by settling and centrifugation. Settled onto glass slides, clay fractions were analyzed air-dry and after saturation with ethylene glycol. Semi-quantitative determination of clay mineral abundances was performed using the method of Biscaye (1965). Chemical composition of the <0.2 μm fraction was determined by EDS microprobe analysis operated at 15 kV and using biotite as a calibration standard. Suspensions of the <0.2 μm fraction were settled onto graphite stubs in order to provide smooth surfaces for microprobe analysis and were then coated by graphite. Morphological characterization of sediments and oxyhydroxides was performed using a Jeol JSM-840 scanning electron microscope (SEM) equipped with an IXRF EDS analytical X-ray system operated at 15–20 kV. Carbon coated specimens of sediments and oxyhydroxides were examined in both secondary and back scattered electron mode. The back scattered images were further processed with Image Pro Plus software in order to determine the cumulative percentages of sulfides and barite in the samples.

4. RESULTS

4.1. Mineralogy and morphology of oxyhydroxide deposits

4.1.1. Oxyhydroxides and oxidized sulfides at the Main Endeavour field

Slightly oxidized sulfides (R710-15) sampled from the foot of a scarp below a chimney structure in the Main Endeavour field are a product of mass wasting of sulfide chimneys. The sulfidic sediment reflects the original chimney mineralogy and consists of pyrite, chalcopyrite, isocubanite, sphalerite, marcasite and pyrrhotite. The sample also contains flaky aggregates of nontronite and native sulfur. The deposits recovered from ponds in an oxidized sulfide mound southeast of the Main Endeavour field (R714-12 and R714-13) are dominantly composed of X-ray amorphous Fe-oxyhydroxide + silica, as shown by XRD and SEM–EDS analyses. Reflections characteristic of poorly crystalline ferrihydrite were not unequivocally detected. This material is hereafter referred to as oxyhydroxide. Other minor phases are barite, quartz and feldspar. Filamentous talc aggregates, which are probably residual chimney material, were also found in R714-13. Oxyhydroxide deposits contain fragments of oxidized sulfides, more abundant in R714-13. The surfaces of the deposits are covered by a thin layer of siliceous ooze containing fragments of radiolarian and diatom tests.

The red oxyhydroxide deposits contain globules and rare straight filaments, which are locally traversed by laminae of dense material that has a flinty dark red appearance (Fig. 2a). Towards the laminae, the globules are coated by a thin layer of amorphous material and appear to be highly degraded. The globules, filaments and flinty laminae are composed of Fe-oxyhydroxide + silica with small amounts of P, Ca and S. The formation of the laminae may have resulted from continued passage of hydrothermal fluids that initially precipitated Fe and Si as globules and filaments. A similar looking red flinty veinlet traversing filaments of possible microbial origin in oxyhydroxide deposits from Woodlark basin has been described by Binns et al. (1993). In the orange oxyhydroxide deposits, Fe-oxyhydroxide + silica occurs as aggregated flaky particles (Fig. 2b). Some of the particles contain, in addition to Fe and Si, S as well as minor Mn, Zn and Cu. Surfaces of the sulfide fragments in the oxyhydroxide deposits are corroded and coated by a fine network of blue and red particles. SEM analysis revealed corrosion pits of rounded shape and a diameter of about 0.5 μm on surfaces of sulfide grains (Fig. 2c). Highly corroded grains transform to fine-grained particles of sulfide composition (Fig. 2d). The corrosion features resemble bacterial leaching patterns observed on the surfaces of pyrite crystals (Bennett and Tributsch, 1978; Mustin et al., 1992) and colloform iron sulfides of chimney structures (Verati et al., 1999).

4.1.2. Oxyhydroxide deposits at the Mothra vent field

At the Mothra hydrothermal field, only approximately 1 cm of the surface of a seafloor deposit could be sampled (R851) and the thickness of the deposit or the underlying substrate is unknown. The deposit is orange with some darker layers and consists of X-ray amorphous Fe-oxyhydroxide ± Mn + silica, as revealed by XRD and SEM–EDS. Reflections characteristic of ferrihydrite were not registered. Other minor phases are barite and quartz. The deposit is coated with a thin layer of siliceous ooze. Morphological studies show a variety of unique microtextures that resemble mineralized microorganisms. Common are filaments that are morphologically similar to filamentous bacteria described in other present and past oxyhydroxide deposits (Juniper and Fouquet, 1988; Edwards et al., 2003; Kennedy et al., 2003); (Fig. 3a, c and d). Less common are rods about 20 μm long and 10 μm wide (Fig. 3b) and globules ranging in diameter from 5 to about 20 μm, some with a hollow interior (Fig. 3c and d). The filaments and rods are dominantly composed of Fe-oxyhydroxide + silica, while the majority of the globules is enriched in Mn (Fig. 3e and f). Manganese-oxide containing Zn and Cu also occurs as flaky aggregates (Fig. 3b and d). Some of the surfaces are covered by a gel-like layer of Fe-oxyhydroxide + silica (Fig. 3a).

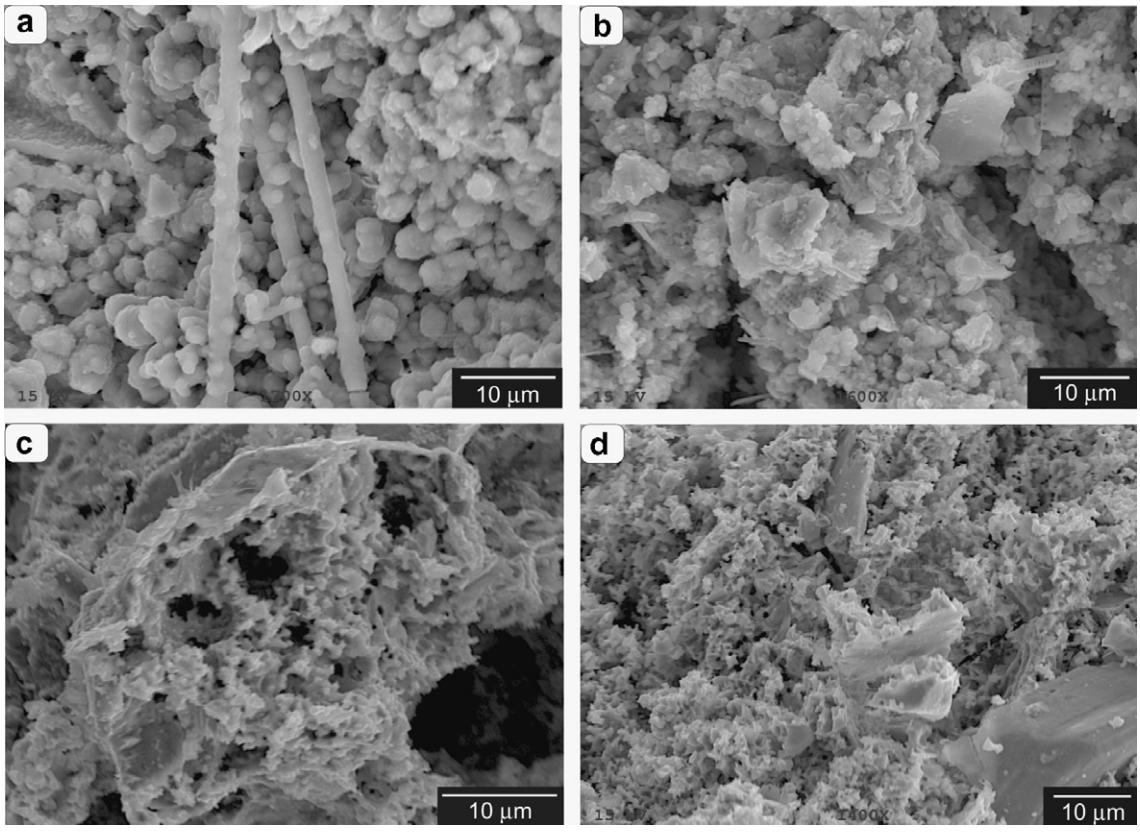

Fig. 2. SEM images of oxyhydroxide deposit at the Main Endeavour field. (a) Globules and filaments composed of Fe-oxyhydroxide + silica. (b) Flaky aggregates of Fe-oxyhydroxide + silica, barite and biogenic detritus. (c) Corroded chalcopyrite constituting oxidized chimney fragment in the oxyhydroxide deposit. The surface is etched by corrosion pits of rounded shape and transformed into fine-grained sulfidic particles. (d) Fine-grained sulfidic particles covering corroded surfaces of sulfides.

The oxidized crust on the external surface of an extinct pyrite–barite–amorphous silica chimney at the Mothra field is up to 1 mm thick and varies in color from red to brown with some yellow patches (R711). The crust consists of X-ray amorphous material of Fe–Si–Mn–S–P–Zn composition, which may represent a mixture of amorphous oxyhydroxides, silica and sulfates, as has been found at Pito seamount as an external layer on chimney fragments with similar composition (Verati et al., 1999). Manganese-oxide enriches the outermost dark brown surface of the crust. Also present are grains of native sulfur that probably account for the yellowish coloration of the crust. The amorphous material of the crust coats pyrite or marcasite globules, pyrrhotite crystals, barite and colloform silica. In places, the amorphous material is dense and macroscopically has the appearance of flinty laminae similar to those observed in the oxyhydroxide deposits at the Main Endeavour field. Within the crust, a variety of unique microtextures that could be biogenic was observed. Figs. 4 and 5 show SEM images of various microtextures including rods (Fig. 4a and b), filaments (Fig. 5a–c) and globules (Fig. 4c and 5d). Imprints of various shapes and sizes that may be relict microorganisms occur within a dense amorphous layer (Fig. 4a and c).

4.2. Mineralogy and morphology of near-vent and ridge flank sediments of the Endeavour segment

4.2.1. Near-vent sediments

Near-vent sediments occur in small ponds and as a thin cover on basalt surfaces. The two sediment samples studied are within 35 m (R849-1) and 200 m (R849-2), respectively, of an actively venting black smoker structure in the central part of the Main Endeavour field. The sediments are yellowish-brown. XRD analysis indicates the presence of large amounts of X-ray amorphous material and variable amounts of smectite, chlorite, quartz, feldspar, calcite, barite and pyrite. SEM–EDS shows that the X-ray amorphous material largely consists of basalt glass fragments, more abundant and larger (up to 3 cm) in R849-1, biogenic detritus and aggregates of variable composition. The biogenic detritus comprises abundant radiolarian tests at different stages of preservation, Si spicules and diatoms. Calcium tests of foraminifera were not found. Most of the radiolarian tests are altered and pores are filled by fine-grained particles (Fig. 6a). In some instances, the entire surface of the radiolarian is covered by fine-grained particles obscuring the original morphology. The near-vent sediments contain disseminated aggregates that are dark brown and black under a light microscope. SEM–EDS analysis of the aggregates show that

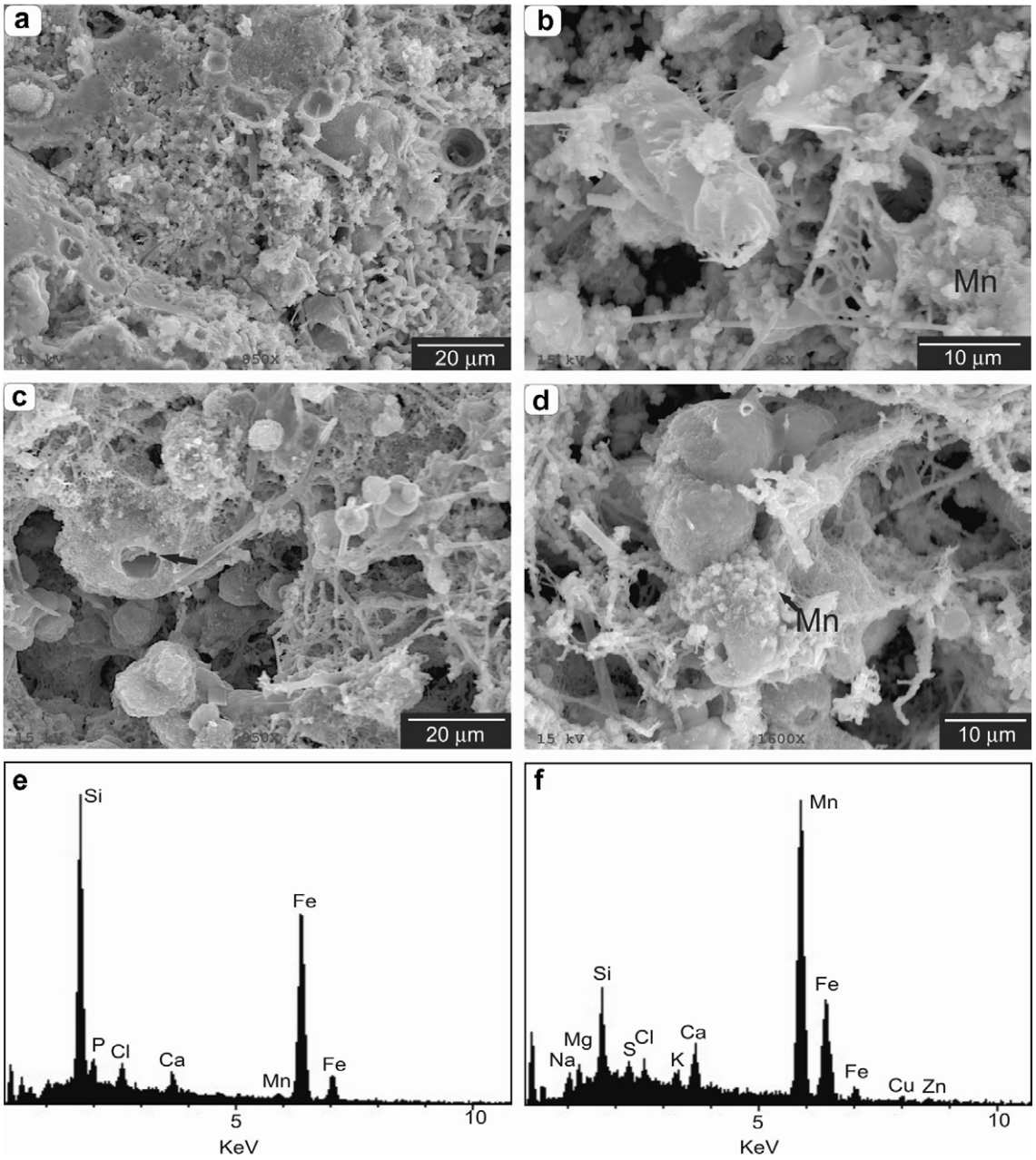

Fig. 3. SEM images of a seafloor oxyhydroxide deposit at the Mothra vent field. (a) Microtexture of the deposit showing filaments and rods composed of Fe-oxyhydroxide + silica that are coated by an amorphous layer of similar composition. The EDS spectra are as that in 3e. (b) Mineralized microbe-like rod and a flaky aggregate of Mn-rich oxyhydroxide (Mn). (c) Mineralized globules of variable size and filaments. The large globule has a hollow interior (arrow). Globules are composed of Fe-oxyhydroxide + Mn + silica. (d) Mineralized filaments and globules and a flaky aggregate of Mn-rich oxyhydroxide (Mn). (e) EDS spectrum of filaments and rods. (f) EDS spectrum of globules and flaky aggregates.

they consist of gel-like material enriched in Mn, Fe and Si and containing minor Ca, Mg, P, Cu and Zn, which is commonly aggregated with fine-grained particles of similar composition, fine-grained sulfides, barite and biogenic debris (Fig. 7a, b, e, and f). Material of similar composition also occurs as aggregates of globular morphology (Fig. 7c), coatings on surfaces of silica spicules (Fig. 6b), as well as encrustations on filaments (Fig. 7d). A common component of the sediments is amorphous material of Fe–Si ± S composition containing minor Ca, Mg and P (Fig. 6d). Sulfides in the near-vent sediments occur as crystalline and colloform aggregates as large as 300 µm and as fine-grained particles less than 10 µm (Fig. 6c). Their compositions are S–Fe, S–Fe–Cu and S–Fe–Cu–Zn, the latter probably representing a mixture of different sulfide phases. Fe-sulfide was also observed as framboids of micron-size particles and globules. Large sulfide particles from 50 to 300 µm in length occur in minor amounts (<1% by visual estimate) only in sample R849-1.

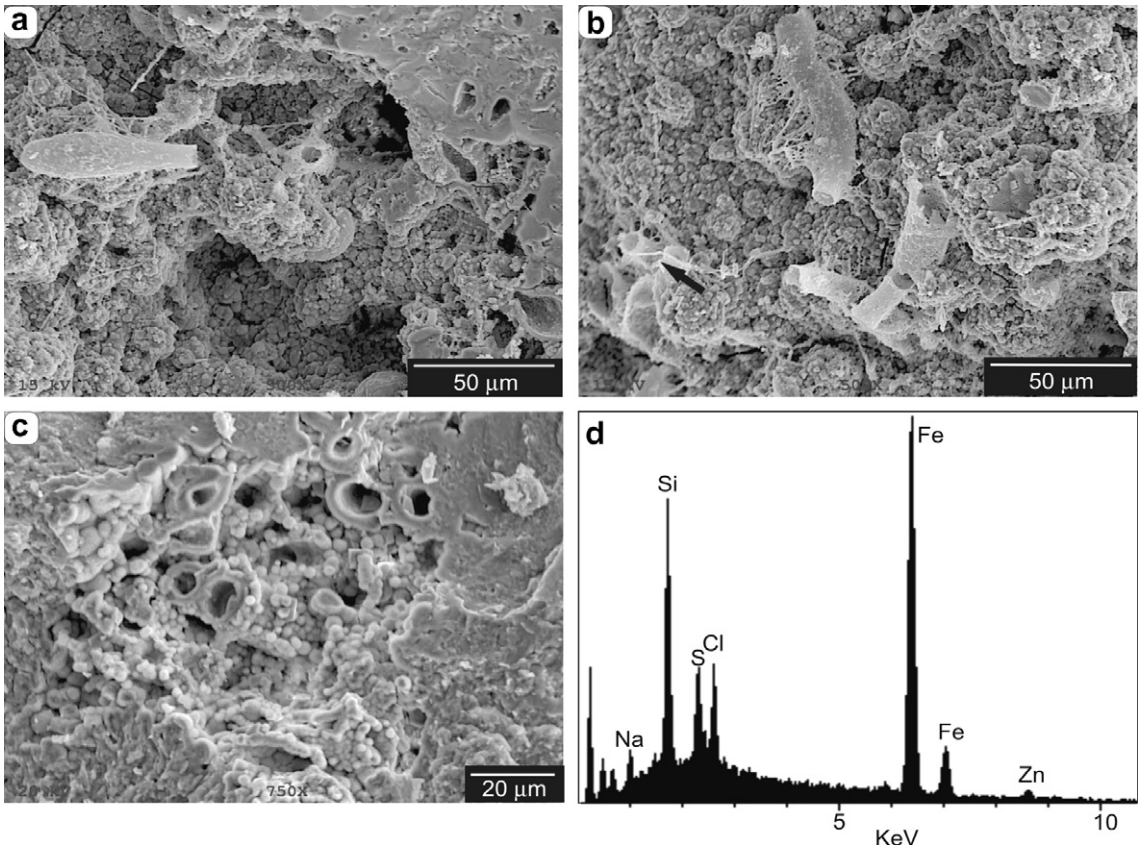

Fig. 4. SEM images and EDS spectrum of an external crust of an extinct chimney at the Mothra vent field. (a) Mineralized rod shaped microorganism attached to an amorphous substrate and imprints in a dense amorphous layer (to the left). (b) Mineralized sheaths of rod shaped microorganisms attached to and embedded (arrow) in an amorphous substrate. (c) Round imprints and globules in dense amorphous material constituting flinty laminae. (d) EDS spectrum of mineralized microorganisms and amorphous material.

Image analysis shows that the total sulfide content of sample R849-1 is approximately 4 percent. In the sediment 200 m from the vent (R849-2), sulfides are predominantly less than 10 μm in size and constitute less than 2 percent of the sediment. Barite occurs as individual and aggregated platy crystals as large as 40 μm in size and as fine-grained particles. Talc is also present in the near-vent sediments as flaky aggregates.

4.2.2. Ridge flank sediments

Sediments within 3 km east and west of the Endeavour ridge axis are hemipelagic clayey silts containing 32–37 wt% of <4 μm fraction. Sediments forming a thin layer on basalt surfaces (R713-3 and R713-4) are brownish-gray, whereas the color of those taken by push corer (R713-1, R732-1 and R732-2) gradually changes from brownish-gray in the upper 0–12 cm interval to olive-gray downwards. The color change reflects a decrease in oxidation of sediments with depth. Sediments consist of smectite, illite, chlorite, quartz, feldspar, calcite, barite, Fe–Mn oxyhydroxide and biogenic detritus. The biogenic detritus is comprised of tests of foraminifera, radiolarians and diatoms. The bulk mineral composition and the clay mineral abundances of the surface sediments and the sediments as deep as 20 cm are quite uniform. Semi-quantitative XRD analysis of the <2 μm fraction shows that smectite is the dominant clay mineral, constituting about 60–66% of the fraction, followed by illite (20–26%) and chlorite (14–17%). Chemical analysis of the <0.2 μm fraction composed of smectite with traces of chlorite shows elevated Fe and low Al concentrations. The chemical composition of the fraction <0.2 μm is in Table 1 together with Fe-rich smectites from other areas. The following structural formula was calculated on the basis of the chemical data with all iron assigned as Fe^{3+}:

$$(Na_{0.61}\ K_{0.37})(Fe_{0.75}\ Al_{0.38}\ Mg_{0.51}\ Ti_{0.02}\ Ca_{0.3})(Si_{3.88}\ Al_{0.12}) \times (O_{10}(OH)_2)$$

The smectite is Fe-rich montmorillonite, as the layer charge originates from the octahedral sheet with iron as a major cation (Güven, 1988). Fe-rich montmorillonite also contains high amounts of Mg and Ca in the octahedral sheet. All of the Ca content was assigned to the octahedral sheet in order to balance the layer charges. The Fe/Si ratio (0.26) of the Fe-rich montmorillonite at Endeavour is similar to that of Fe-rich montmorillonite from the northeast to southeast Pacific (Aoki et al., 1974; Aoki et al., 1979) and the DOMES area in the equatorial Pacific (Hein et al., 1979).

4.3. Mineralogy of sediments at Nootka mud volcano

Sediments were sampled at Nootka mud volcano as a background far removed from the hydrothermal influence

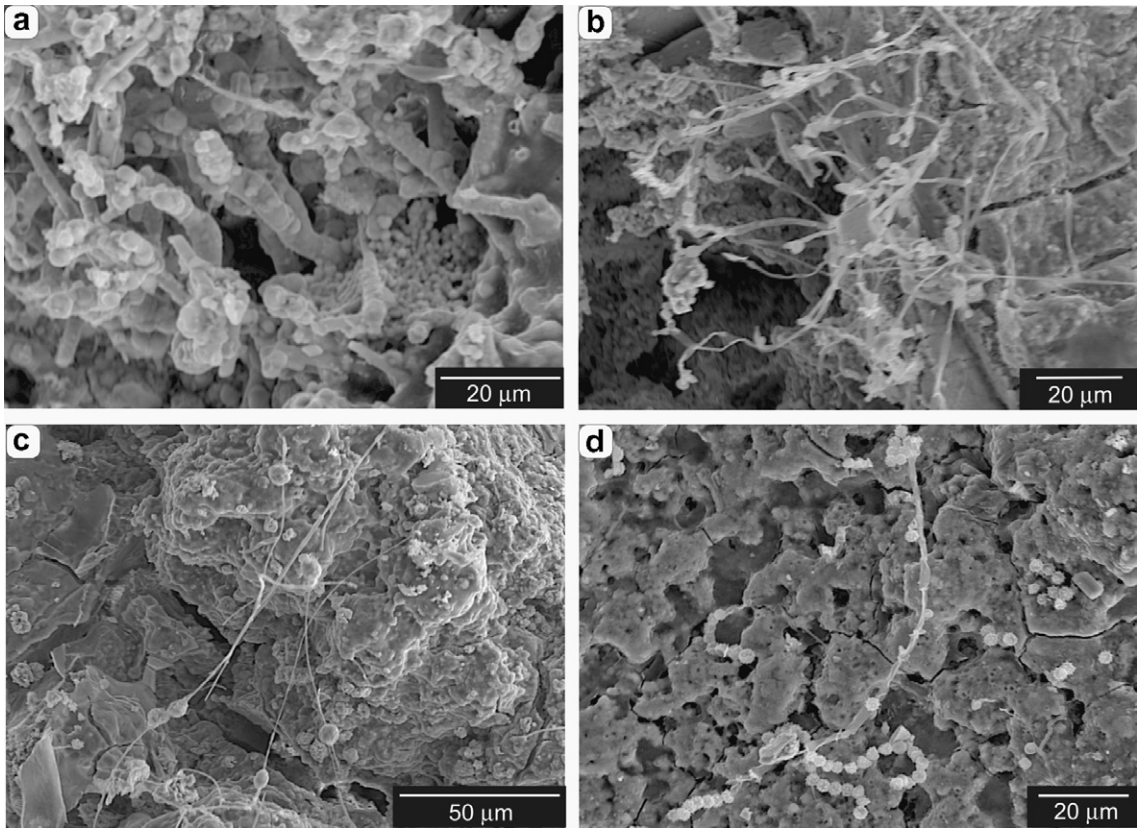

Fig. 5. SEM images of an external crust of an extinct chimney at the Mothra vent field. (a) Filaments coated by mineral precipitate. (b) Mineralized fine branched filaments with "grapes" at the end. (c) Mineralized fine filaments connecting oval bodies. Some of the oval bodies are embedded in an amorphous substrate. (d) Mineralized globules that form chains or are attached to a fine filament on the outer surface of the chimney crust.

at Endeavour. However, there could be other, closer, still unknown, hydrothermal source. Hemipelagic sediments taken to 20 cm depth are silts containing up to 28 wt% of <4 μm fraction. Nootka sediments have higher amounts of quartz and feldspar than the ridge flank sediments of Endeavour as a result of more abundant detrital supply. The amount of detrital chlorite in the fraction <2 μm is also slightly higher (19–21%) here and the amount of detrital illite is similar to that at Endeavour. As in the Endeavour sediments, smectite is the dominant clay mineral, constituting between 55% and 60% of the <2 μm fraction. The chemical analysis of the <0.2 μm fraction shows higher Al concentration and less Fe than that at Endeavour (Table 1). The chemical composition could be a result of a mixture of two types of smectite, Fe-rich montmorillonite and beidellite. Traces of illite could also contribute to higher Al content.

4.4. Major and trace element geochemistry

4.4.1. Major elements

The bulk geochemical composition of representative samples is presented in Table A1. Concentrations of Fe_2O_3 in Endeavour sediments decrease from 25.22 wt% near the vents to 9.25 wt% on the ridge flanks. The near-vent sediments and oxidized surface sediments of the ridge flanks are also enriched in Mn (0.72–1.27 wt% MnO), whereas the ridge flank sediments from deeper intervals have lower Mn contents. The upward increase of Mn concentrations in the ridge flank sediments is not accompanied by an increase in concentrations of other metals and likely reflects diagenetic mobilization and redeposition of Mn in the oxidized surface layer. The relative contribution of hydrothermal and detrital components in oxyhydroxides and sediments at Endeavour and Nootka is presented in an Al/(Al + Fe + Mn) versus Fe/Ti plot (after Boström and Peterson, 1969, and Peter and Goodfellow, 1996; Fig. 8). Shown also are East Pacific metalliferous sediments from areas of high heat flow on the crest of the EPR and from areas of average to low heat flow east and west of the rise (Boström and Peterson, 1969), North Pacific pelagic sediment (Kyte et al., 1993) and terrigenous sediment from the Middle Valley, Juan de Fuca Ridge (Goodfellow and Peter, 1994). The Endeavour samples lay on a mixing curve between pure East Pacific metalliferous sediments and North Pacific pelagic sediments.

The oxyhydroxide deposits at the Main Endeavour field and Mothra are compositionally similar to the metalliferous sediments in areas of high heat flow on the crest of the EPR. Despite their proximity to high heat flow, near-vent sediments of the Main Endeavour field plot closer to the average to low heat flow EPR metalliferous sediments.

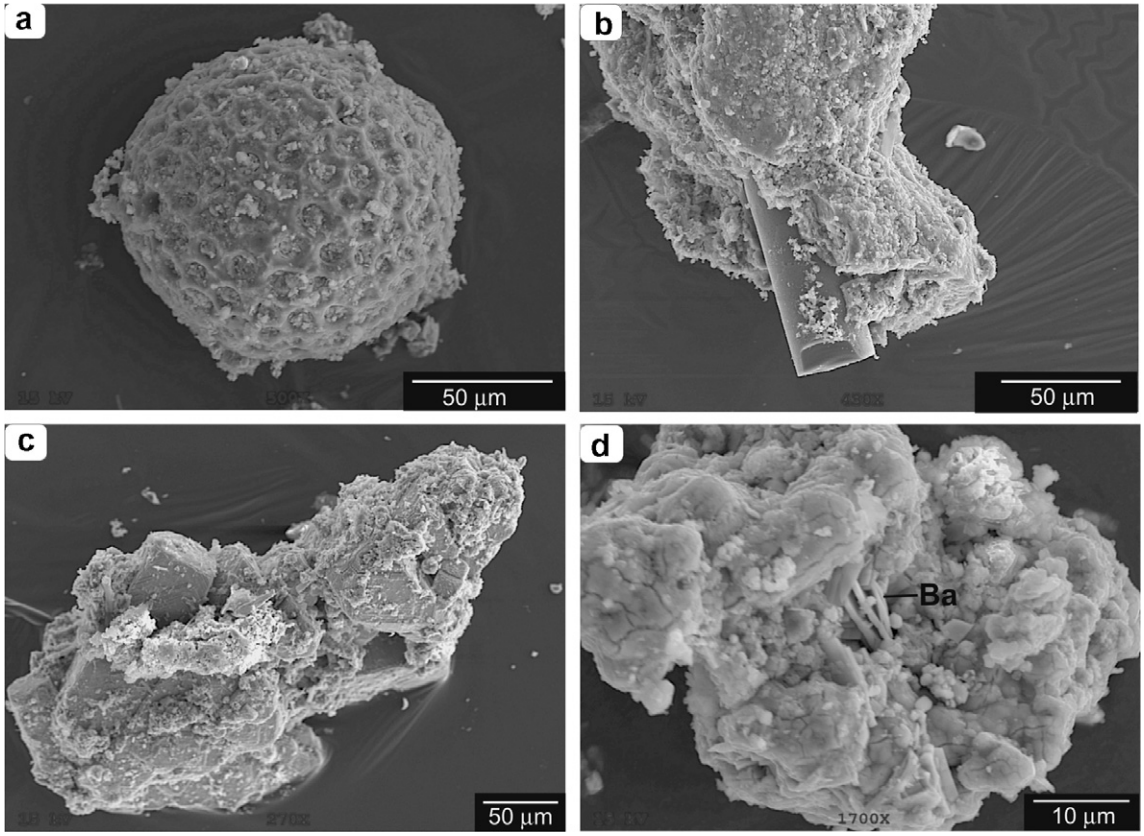

Fig. 6. SEM images of near-vent sediments of the Main Endeavour field. (a) Altered radiolarian test with pores filled by fine-grained particles. (b) Amorphous material of Mn–Fe–Si–Ca–Cu composition coating a silica spicule. (c) Aggregate of pyrite crystals. (d) Aggregate of gel-like material of Fe–Si–S composition and platy barite crystals (Ba).

The shift towards a more detrital composition is a consequence of contamination by basaltic fragments and terrigenous components. The terrigenous input is more pronounced in the ridge flank sediments, which is reflected in their position on the mixing curve towards North Pacific pelagic sediments in Fig. 8. Nootka sediments, being dominantly of terrigenous origin, plot in the field for the Middle Valley terrigenous sediments.

In the oxyhydroxide deposits at the Main Endeavour field and Mothra, concentrations of SiO_2 are between 20.11 and 38.67 wt%, which is much higher than concentrations of SiO_2 in other oxyhydroxides associated with sulfides (Hekinian et al., 1993). The values of SiO_2 concentrations are more relevant to Fe–Si oxyhydroxide deposits primarily precipitated from low-temperature fluids (Puteanus et al., 1991; Hekinian et al., 1993; Scholten et al., 2004). In Endeavour sediments, Si resides in siliceous tests, authigenic Fe-rich montmorillonite, detrital aluminosilicates, quartz and basalt fragments. An additional source of Si in the near-vent sediments is amorphous Fe–Si-rich phases deposited from the hydrothermal plume. Calcium content in sediments is largely controlled by the presence of calcareous foraminifera tests. The elevated concentrations of CaO in the ridge flank sediments are related to their presence, while low Ca concentrations in the near-vent sediments of Endeavour and sediments of Nootka is a consequence of their absence. High concentrations of P_2O_5 (up to 3 wt%) are found in oxyhydroxides and near-vent sediments, all of which contain abundant Fe-oxyhydroxide (Fig. 9a). Good correlation between P and Fe characterizes Fe-rich sediments and suspended matter of hydrothermal plumes and has been attributed to scavenging of P from seawater by colloidal Fe-oxyhydroxides (Feely et al., 1992, 1994). Another source of P in modern pelagic sediments is apatite of biogenic origin, but SEM–EDS analysis of Endeavour samples did not reveal its presence. Some of the Fe-oxyhydroxide + silica also contain Ca; however, the bulk content of P_2O_5 relative to CaO exceeds the ratio for apatite. Sulfur content is related to a large extent to the presence of sulfide phases. Low concentrations of S in both near-vent (0.9–2.2 wt%) and ridge flank sediments (0.1 wt%) reflect scarcity of sulfides. Normative analyses that match concentrations of S with those of Fe and Ba show that the sulfur content accounts for a maximum of 3% pyrite in the sediment deposited within 35 m of an active vent (R849-1); the rest of Fe is present as oxyhydroxide (M.P. Gorton, personal communication).

4.4.2. Trace elements

Distribution of the concentrations of Cu, Zn, Ba, and Mn is shown in Fig. 1b. Variations in the concentrations of As, Mo and Pb in samples as a function of hydrothermal and detrital content are illustrated in element versus Fe/Ti plots (Fig. 9). The maximum concentrations of Cu

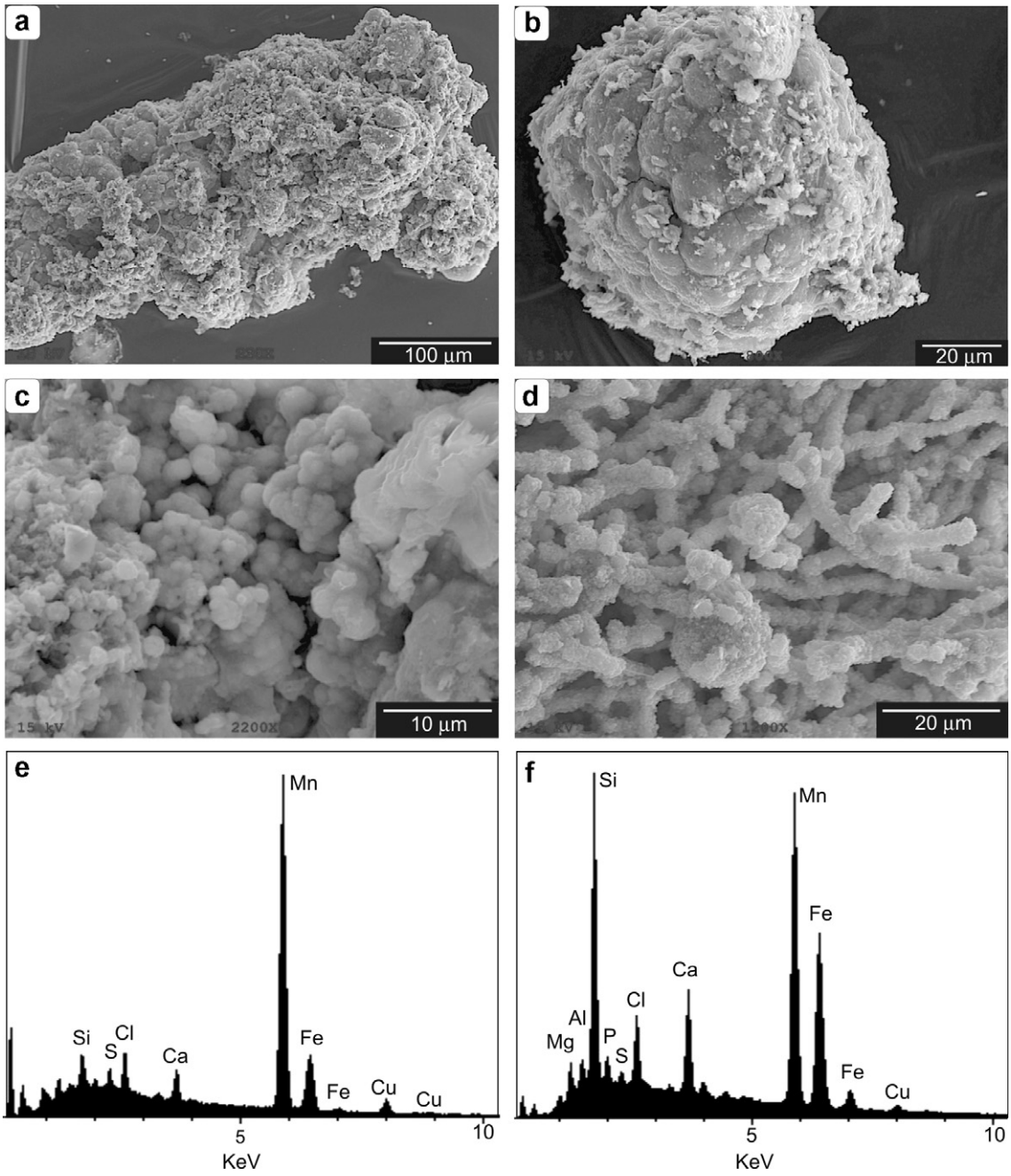

Fig. 7. SEM images and EDS spectra of near-vent sediments of the Main Endeavour field. (a) Aggregate of gel-like material enriched in Mn-oxide and fine-grained particles. The EDS spectrum of the gel-like material is similar to that in Fig. 3e. (b) Gel-like material of globular morphology and Mn–Fe–Si–Ca–Cu composition. (c) Globular aggregate with EDS spectrum similar to that in Fig. 3e. (d) Mineralized filaments and globules with a spectrum similar to that in Fig. 3f. (e) EDS spectrum of amorphous material. (f) EDS spectrum of amorphous material.

(5.3 wt%) and Zn (1.5 wt%) are in the sulfidic sediment. With respect to their Cu and Zn content (total Cu + Zn up to 2.1 wt%), the oxyhydroxide deposits at the Main Endeavour field are analogs of secondary oxyhydroxides associated with weathered sulfides (Hekinian et al., 1993). The metal content of the Mothra oxyhydroxide deposit (Cu + Zn = 5470 ppm) is higher than that in primary oxyhydroxide deposits from other locations (Puteanus et al., 1991; Binns et al., 1993; Hekinian et al., 1993; Scholten et al., 2004) and may indicate that it was formed in proximity to sulfides (Boyd et al., 1993). Lead is preferentially enriched in oxyhydroxides rather than in sulfides (Table A1; Fig. 9d). Lead contents in the Endeavour oxyhydroxides are much higher than Pb contents reported for other primary and secondary oxyhydroxide deposits (Binns et al., 1993; Boyd et al., 1993; Scholten et al., 2004) and are closer

Table 1
Chemical composition of <0.2 μm fraction of sediments from the Endeavour segment and Nootka and of iron-rich smectites reported in the literature

Sample	SiO_2 (wt%)	Al_2O_3 (wt%)	TiO_2 (wt%)	Fe_2O_3 (wt%)	MnO (wt%)	MgO (wt%)	CaO (wt%)	K_2O (wt%)	Na_2O (wt%)
Endeavour segment	43.7	4.8	0.3	11.3	n.d.	3.8	3.2	3.3	3.5
Nootka	45.7	12.1	0.5	8.3	n.d.	2.4	1.2	2.7	0.8
NE Pacific[a]	51.3	7.4	1.0	14.6	0.2	4.2	0.5	0.7	1.3
SE Pacific[b]	50.2	7.1	0.8	11.5	0.1	5.4	0.3	0.6	2.9
Bauer Deep[c]	49.7	5.0	0.2	17.9	0.4	4.5	0.3	0.6	1.3

n.d., not determined.
[a] Aoki et al. (1974).
[b] Aoki et al. (1979).
[c] Cole (1985).

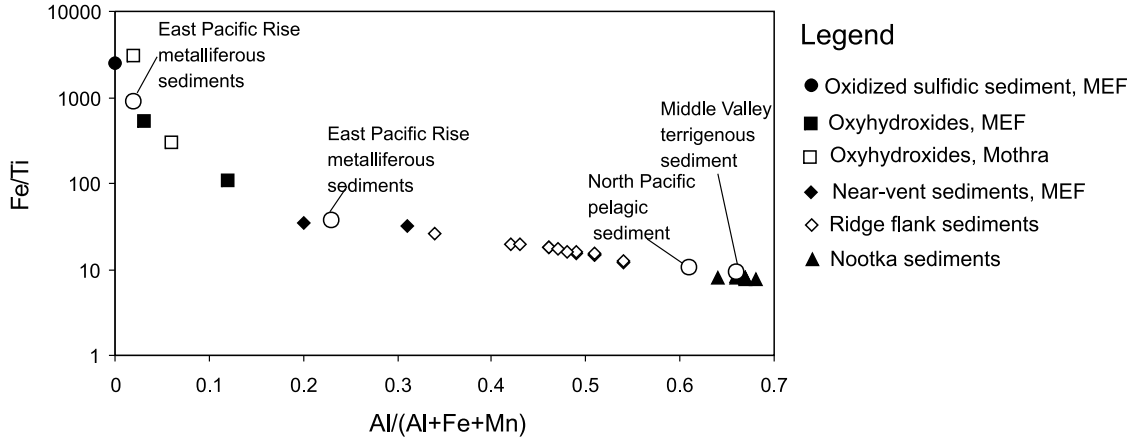

Fig. 8. Plot of Fe/Ti versus Al/(Al + Fe + Mn) illustrating variations in the amount of hydrothermal and detrital components of samples from Endeavour and Nootka. Shown also are East Pacific Rise metalliferous sediments (Boström and Peterson, 1969); North Pacific pelagic sediment (Kyte et al., 1993); and terrigenous sediment from Middle Valley, Juan de Fuca Ridge (Goodfellow and Peter, 1994).

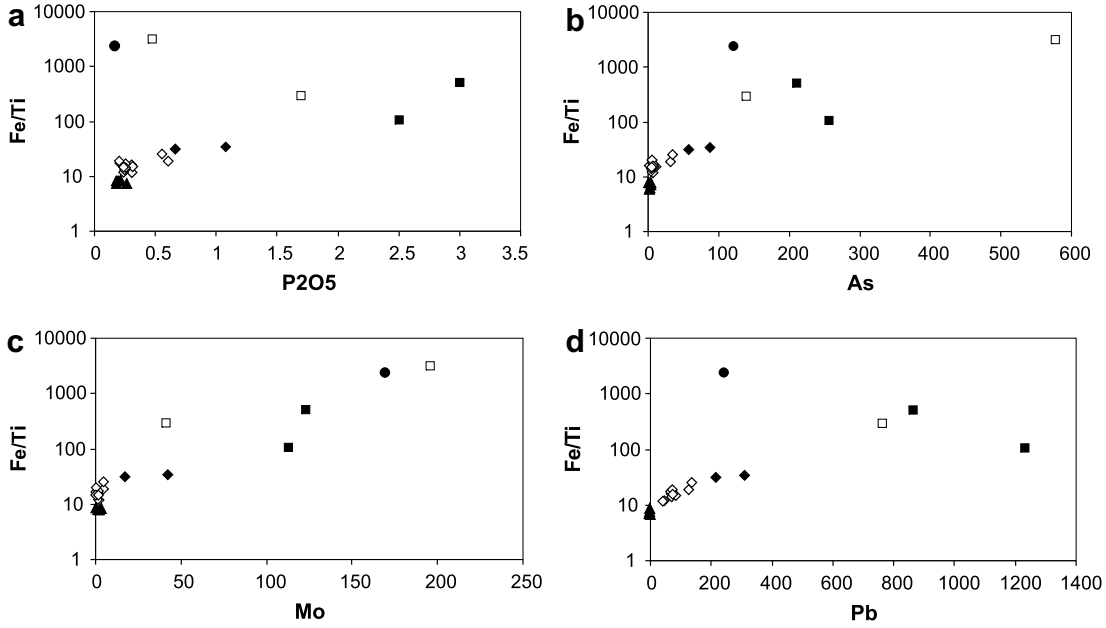

Fig. 9. Plots of concentrations of (a) P_2O_5, (b) As, (c) Mo and (d) Pb versus Fe/Ti. Plots illustrate distribution of elements as a function of varying amounts of hydrothermal and detrital components of samples from Endeavour and Nootka. Legend is as in Fig. 8.

to those in hydrogenous deposits (Hein et al., 1999). However, unlike hydrogenous deposits, Pb enrichment in oxyhydroxide phases at Endeavour does not correlate with enrichment of Mn, Co and Ni. Both sulfide and oxyhydroxide phases at Endeavour are enriched in As, Mo (Fig. 9b and c) as well as Co and Au (not shown).

Uranium has anomalously high concentrations of up to 30.3 ppm in oxyhydroxides at the Main Endeavour field that are associated with sulfides and low concentrations in oxyhydroxides at Mothra that are not directly associated with sulfides. The chimney crust is also enriched in U (22.9 ppm) in contrast to the sulfide-rich interior, which is depleted in U (3.6 ppm). This distribution of U at Endeavour shows affinity to deposits containing both weathered sulfides and oxyhydroxides. Analogous enrichment of U in sulfide-bearing layers of metalliferous sediments on the Mid-Atlantic Ridge has been attributed to reductive fixation of U derived from seawater at or near the oxide/sulfide boundary of oxidized sulfide particles (German et al., 1993; Mills et al., 1994).

In Endeavour sediments, the concentrations of the trace metals, except for Cr and Ni, as well as As are anomalous relative to the background values in Nootka sediments (Table A1). Concentrations of As (3–89 ppm), Mo (0.5–42 ppm) (Fig. 9b and c) as well as Co (19–76 ppm) (not shown) are elevated only in the near-vent sediments and drop quickly to background levels away from the vents Concentrations of Cu (145–6122 ppm), Zn (200–1907 ppm), Pb (43–307 ppm) and Ba (0.3–0.7 wt%), on the other hand, remain above background levels in the ridge flank sediments (Fig. 1b). In sediment cores down to 20 cm depth taken from the ridge flanks, metals, except for Mn, show little fluctuation in their concentrations, thus indicating steady hydrothermal input.

4.5. Selective leaching

Selective leaching with hot hydroxylamine was performed in order to evaluate the partitioning of metals between oxyhydroxides and a residue consisting of sulfides, sulfates and aluminosilicates. Hot hydroxylamine leach attacks amorphous and crystalline Fe–Mn oxyhydroxides but not well-crystallized iron oxides. Carbonates also dissolve during hydroxylamine treatment. As XRD analysis does not indicate the presence of detectable amounts of crystalline iron oxides, we consider that sulfides and aluminosilicates are the major residual phases containing metals. We analyzed one near-vent (R849-1) and one ridge flank (R713-3) sediment of the Endeavour segment. The concentrations of metals in the leached fraction that is dominated by Fe–Mn oxyhydroxides are given in Table 2, and Fig. 10 shows their concentrations in Fe–Mn oxyhydroxides as a percentage of the bulk concentrations. Fe–Mn oxyhydroxides constitute up to 20 wt% of the bulk sediments. Concentrations of Fe and Mn in oxyhydroxides are 5.3 wt% and 6370 ppm, respectively, in the near-vent sediment and 2.3 wt% and 5630 ppm, respectively, in the ridge flank sediment. These values are notably less than the values reported by Barrett et al. (1987) for the oxyhydroxide metalliferous component of sediments from the East Pacific Rise. Iron and Cr have higher affinity for residual phases than for oxyhydroxides (15–20% of their total concentrations). In the near-vent sediment, carriers of Fe other than oxyhydroxides are sulfides and aluminosilicate phases, such as authigenic Fe-rich montmorillonite, detrital clays and basalt fragments. The lack of detectable amounts of sulfides in the ridge flank sediment suggests that Fe is largely (85% of the total concentration) in authigenic Fe-rich montmorillonite and detrital clays. Manganese together with Pb and Co is largely in Fe–Mn oxyhydroxides. Lead has the highest affinity for oxyhydroxides, with up to 75% of the total concentration carried by oxyhydroxide phases. In the near-vent sediments, Fe–Mn oxyhydroxides also carry significant portions of Cu (2250 ppm) and Zn (878 ppm), with the rest being in sulfides and possibly Fe-rich montmorillonite. Away from the vents, aluminosilicate phases, Fe-rich montmorillonite in particular, are the dominant carrier of Cu (350 ppm) and Zn (238 ppm).

Table 2
Concentrations of elements in a fraction extracted by hot hydroxylamine leach

Sample	Fe (ppm)	Mn (ppm)	Co (ppm)	Ni (ppm)	Cu (ppm)	Zn (ppm)	Pb (ppm)	Cr (ppm)
Endeavour near-vent sediment (R849-1)	53,400	5630	43	25	2250	878	230	12
Endeavour ridge flank sediment (R713-3)	23,000	6370	13	38	196	166	84	14

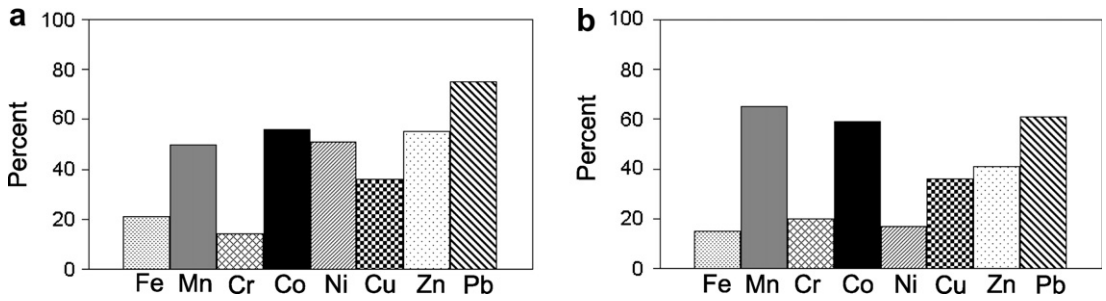

Fig. 10. Concentrations of metals in Fe–Mn oxyhydroxides leached by hot hydroxylamine as a percentage of the bulk concentrations in (a) near-vent sediment and (b) ridge flank sediment.

4.6. Rare earth element geochemistry

The concentrations of rare earth elements are in Table A1. REEs were normalized to both chondrite and North America shale composite (NASC) and the respective representative patterns are shown in Fig. 11. Normalization to NASC was performed in order to reveal positive Eu anomalies in samples containing a terrigenous component. The Eu content of chondrite is within the range of variability of other LREE, while such differences are more pronounced in the NASC, thus emphasizing the Eu anomaly. For the calculation of Ce and Eu anomalies, we used the REE values normalized to NASC. The deviation of Ce from the rest of the REE, known as the Ce anomaly, is calculated after Toyoda and Masuda (1991). In the absence of Gd data, the Eu_n/Sm_n ratio was used to approximate the Eu anomaly, as proposed by Mills and Elderfield (1995).

Chondrite normalized REE patterns of oxyhydroxides at the Main Endeavour field and Mothra show enrichment in LREE, a negative Ce anomaly and a positive to absent Eu anomaly (Fig. 11a). The presence of negative Ce anomalies in the REE patterns of oxyhydroxides together with REE concentrations that are much higher than in hydrothermal fluids indicate that REE composition was modified by scavenging of REEs from seawater (De Baar et al., 1985; Hekinian et al., 1993; Mills and Elderfield, 1995; German et al., 1999; Fig. 11h). The positive Eu anomaly of the REE patterns reflects contribution of hydrothermal material precipitated from high-temperature fluids (Michard et al., 1993; Klinkhammer et al., 1994; Scott, 1997; Fig. 11h). In the oxyhydroxides at the Main Endeavour field, a strong positive Eu anomaly is in the bulk sample (R714-13) containing more abundant chimney fragments of oxidized sulfides and talc. In order to estimate the REE signature of "pure" oxyhydroxide, we selectively analyzed dark red material of sample R714-13, which consists of Fe-oxyhydroxide + silica and does not have chimney fragments. Its chondrite normalized REE pattern exhibits both Ce and Eu depletion suggestive of strong seawater influence on the formation of the oxyhydroxide and is similar to some primary Fe-oxyhydroxides from volcanic seamounts (Hekinian et al., 1993; Scholten et al., 2004; Fig. 11a). A slightly positive Eu anomaly in addition to a negative Ce anomaly characterizes the REE pattern of the Mothra seafloor oxyhydroxide deposit (Fig. 11a).

REE patterns of Endeavour sediments result from variable contributions of plume-derived hydrothermal material, authigenic Fe-rich montmorillonite, detrital aluminosilicates, basalt fragments and biogenic detritus. The chondrite normalized REE patterns show LREE enrichment, slight to absent negative Ce anomalies and slight to absent negative Eu anomalies (Fig. 11b and c). REE patterns with LREE enrichment and negative Eu anomalies characterize the dominantly terrigenous sediments from Nootka (Fig. 11d). An REE pattern with LREE enrichment and a negative Eu anomaly was reported for lithogenic clays of the North Pacific Ocean (Piper, 1974; Fig. 11g), suggesting that the chondrite normalized REE patterns of the sediments reflect major detrital contributions. Normalization to NASC reveals a pronounced negative Ce anomaly and a positive Eu anomaly in the REE pattern of the near-vent sediment deposited within 35 m of the vent (R849-1) (Fig. 11e). The REE pattern is similar to REE patterns of plume particulates (German et al., 1990) and plume-derived hydrothermal sediments (Mills et al., 1993; German et al., 1993; Chavagnac et al., 2005). Away from the vents, the hydrothermal signature is obscured, as is shown by the lack of a pronounced positive Eu anomaly in the near-vent sediment deposited within 200 m of the vent (R849-2) and in the ridge flank sediments (Fig. 11e and f; Fig. 12a). The extent of the negative Ce anomaly in the sediments is largely controlled by the amount of detrital component, as demonstrated in a plot of Fe/Ti versus Ce/Ce^* (Fig. 12b). Detrital input also largely controls Sm and La abundances in sediments. Plots of Fe/Ti versus Sm/Fe and La/Fe mimic that of Fe/Ti versus Al/(Al + Fe + Mn) and show that the increase in concentrations of Sm and La in sediments reflects increasing proportions of detrital material (Fig. 12c and d).

5. DISCUSSION

5.1. Oxyhydroxides

In areas of high-temperature venting and deposition of sulfides, the origin of the associated Fe-rich oxyhydroxide deposits has been attributed essentially to oxidation of sulfides (e.g., Haymon and Kastner, 1981; Hannington et al., 1988; Herzig et al., 1991; Hekinian et al., 1993), while direct precipitation from hydrothermal fluids is less common (Hekinian et al., 1993; Mills and Elderfield, 1995). We suggest that the oxyhydroxide deposits at the Main Endeavour field have a dual origin, oxidation of mound sulfides accompanied by precipitation of primarily Fe-oxyhydroxide + silica from low-temperature fluids. The reasoning for this interpretation is the occurrence of oxidized sulfides within Fe-oxyhydroxides that have silica contents of up to 33 wt% SiO_2, which are uncharacteristically high for secondary oxyhydroxides, and REE patterns with a negative Eu anomaly characteristic of low-temperature hydrothermal fluids (Michard et al., 1993; Scholten et al., 2004). The surveys at the Main Endeavour field have shown that diffuse flow is common both within and distal to the field (Kelley et al., 2001a; Kristall et al., 2006). We consider that the seafloor oxyhydroxide deposit at Mothra was directly precipitated; however, the hydrothermal fluid was probably less diluted with seawater, as indicated by the positive Eu anomaly of the REE pattern. Positive Eu anomalies in REE patterns of Mn crusts from the Pitcairn Hotspot Region have been attributed to periods of extensive high-temperature hydrothermal activity (Scholten et al., 2004). The textural and geochemical characteristics of the oxidized crust of a chimney at Mothra also suggest that it was formed as an external precipitate during the active stage of the chimney rather than as a later oxidation product. A possible mechanism of formation is conductive cooling of the hydrothermal fluids as they travel through the chimney wall and precipitate Fe–Si–Mn–S–Zn phases at the chimney wall/seawater interface. Such a mechanism is in accordance with that proposed for the growth of a diffusely venting sulfide structure at Mothra (Kristall et al., 2006).

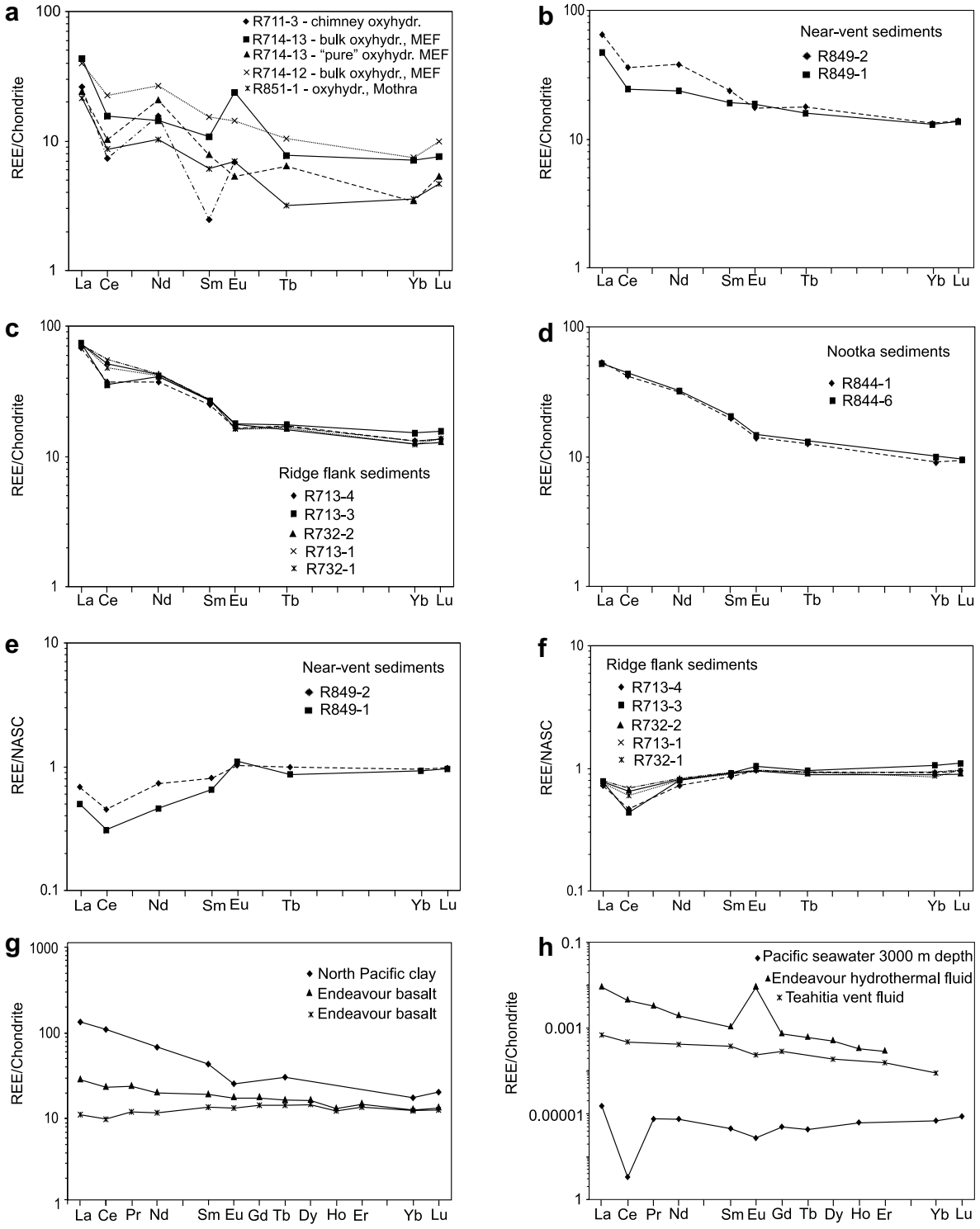

Fig. 11. Chondrite normalized REE patterns of (a) oxyhydroxides at Endeavour, (b) near-vent sediments of the Main Endeavour field, (c) ridge flank sediments of Endeavour, (d) sediments of Nootka. NASC normalized REE patterns of (e) near-vent sediments of Endeavour and (f) ridge flank sediments of Endeavour. Chondrite normalized REE patterns of (g) clay from the North Pacific (Piper, 1974) and two basalts from the Endeavour segment (provided by J. Gill, unpublished data), (h) Pacific seawater (De Baar et al., 1985), Endeavour vent fluid (Klinkhammer et al., 1994) and Teahitia vent fluid (Michard et al., 1993).

The oxyhydroxides at Endeavour exhibit diverse microtextures, some of which resemble those attributed to microbes elsewhere, both modern (e.g., Boyd and Scott, 2001; Edwards et al., 2003; Kennedy et al., 2003) and ancient (e.g., Juniper and Fouquet, 1988), and may indicate the existence of unique microbial populations. As pointed

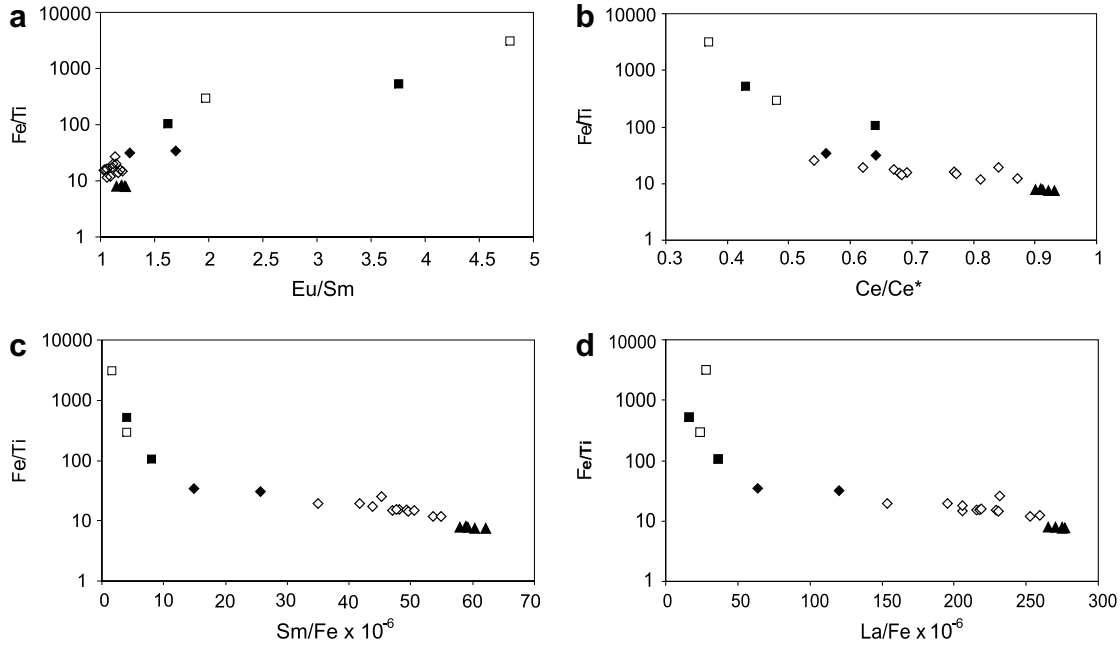

Fig. 12. Plots of Fe/Ti ratio versus (a) Eu anomaly expressed as Eu/Sm, (b) Ce anomaly (Ce/Ce*), (c) Sm/Fe ratio and (d) La/Fe ratio. Plots illustrate variations of REE composition as a function of varying amounts of hydrothermal and detrital components in oxyhydroxides and sediments from Endeavour and Nootka. Legend is as in Fig. 8.

out in other studies, the style of venting at the Endeavour hydrothermal field could support growth of unique microbial communities (Kelley et al., 2001b; Kristall et al., 2006).

5.2. Near-vent and ridge flank sediments

5.2.1. Mineral composition

The mineral composition of the sediments of Endeavour reflects varying contribution of hydrothermal, detrital, authigenic and biogenic inputs. The hydrothermal phases in the sediments are exclusively derived from plume fallout and their dispersal is controlled by factors such as plume dynamics, ridge topography and currents. We cannot assess adequately the effect of all these factors due to limitations of the sampling. However, our study is the first at Endeavour to compare the composition of near-vent and ridge flank sediments to that of particulate matter in buoyant and neutrally buoyant plumes. Our observations show that the composition of near-vent sediments of the Main Endeavour field differ significantly from that of black smoker particles of the buoyant plume at Endeavour, reported in other studies. The major differences are the absence of anhydrite, scarcity of sulfides and the presence of Fe–Si ± S- and Mn–Fe–Si-rich phases in the near-vent sediments. Feely et al. (1987) found that the black smoker particles of the buoyant plume at the Endeavour segment were primarily composed of anhydrite, chalcopyrite, sphalerite, barite, sulfur, pyrite and other less abundant sulfides, ranging in size from <10 to 500 μm. Dymond and Roth (1988) analyzed plume particles collected with moored sediment traps 2 km northeast of the Main Endeavour hydrothermal field and found anhydrite, barite, chalcopyrite, pyrite, sphalerite, elemental sulfur, quartz, 15–16 Å clay mineral and oxides. Sulfides comprised up to 41% of the hydrothermal material and occurred as large non-aggregated grains as well as ~2 μm grains aggregated with biogenic debris. Dymond and Roth (1988) interpreted the presence of large sulfide particles away from the Main Endeavour field to be a result of another major field in the vicinity of the mooring site. This was probably the later discovered High Rise vent field.

The absence of anhydrite in the sediments can be explained by dissolution of anhydrite that, according to Feely et al. (1987), takes place within the water column. Feely et al. (1987) have also shown that dissolution of sulfides may occur at the seawater–sediment interface. Dissolution of sulfides may account to some extent for the scarcity of sulfides in the near-vent sediments as opposed to their abundance in the buoyant plume. Though some of the fine-grained sulfides may have dissolved, the coarser-grained sulfides do not exhibit evidence of dissolution. Furthermore, dissolution processes cannot explain the presence of fine-grained (<10 μm) sulfides and the absence of coarser-grained (>50 μm) sulfides in sediment deposited within 200 m of an active black smoker, as it would be expected that fine-grained sulfides would dissolve first leaving more resistant coarser-grained sulfides. The distribution pattern of sulfides in the near-vent sediments appear to mainly reflect processes of initial aggregation and settling from the plume and indicate that the majority of the large sulfide grains have settled in the vicinity of the vent. This observation is in agreement with models of Feely et al. (1987, 1994) for vents of the Juan de Fuca Ridge predicting that deposition of large sulfide particles (>100 μm) should occur near the vents. The early deposition of sulfides at Endeavour is supported by the fact that only fine sulfide grains, ranging from <0.5 to about 2 μm in size, were found in the neutrally

buoyant plume within the ridge axis (Feely et al., 1992). Our study shows that, besides large sulfide particles, some fine-grained sulfides were also deposited near the vents, possibly as aggregates with lithic and biogenic particles. Agglomeration of fine particles was considered largely responsible for the sharp decrease in transmission anomaly observed for the Endeavour hydrothermal plume (Kadko et al., 1990). One mechanism of aggregation, as suggested by Dymond and Roth (1988) for near-field suspended particulate matter at the Endeavour segment, could have been zooplankton filtration and settlement of particles as fecal pellets. Another possible mechanism of agglomeration is attachment of particles to reactive surfaces such as hydroxides, dissolving silica tests or bacteria.

The presence of Fe–Si ± S- and Mn–Fe–Si-rich phases is another characteristic feature of the near-vent sediments of the Main Endeavour field. Phases of similar composition were not reported in the plume particulates of the Endeavour field (Feely et al., 1987; Dymond and Roth, 1988). However, Feely et al. (1987) reported unidentified Fe–Si and Ca–Si phases and Fe-oxyhydroxides in the black smoker plume of the southern Juan de Fuca Ridge. The authors also observed that iron and silicon phases were prime components of the near-vent hydrothermal sediments, with iron being largely in the form of amorphous oxyhydroxide. The mineral assemblage was considered to be consistent with conductive cooling of vent fluids, as opposed to the studied vents of the Endeavour segment where mineral assemblages were considered to be indicative of high-temperature reaction during mixing between vent fluids and seawater. The occurrence of phases containing silica, Fe and Mn oxyhydroxides and possibly sulfates in the studied near-vent sediments of the Main Endeavour field could be a local phenomenon, determined by the style of venting of the nearby structures, i.e., high-temperature mixing reaction with seawater and/or conductive cooling of vent fluids. Conductive cooling of hydrothermal fluids and ammonia buffering of the pH allows precipitation of amorphous silica phases and facilitated growth of large structures at Endeavour (Tivey and Delaney, 1986; Tivey et al., 1999). Local biogenic productivity may have also been a factor in the formation and deposition of the amorphous phases, as microorganisms may have provided reactive surfaces and enhanced chemical precipitation of elements. Straube et al. (1990) have provided evidence for the existence of unique microbial populations heterogeneously distributed in hot buoyant plumes at the Endeavour segment.

In the near-vent sediments of the Main Endeavour field, Mn-rich amorphous material occurs as distinct aggregates apparently settled from the plume. This suggests that a portion of the Mn was precipitated during early stages of the plume dispersal together with Fe and Si. Mn-rich amorphous material contains also Cu and Zn that were probably absorbed by Mn oxides during dispersal of the plume. In reducing hydrothermal fluids, manganese is present as dissolved Mn(II) that has a slower rate of oxidation than iron. The non-conservative behavior of some of the Mn suggested by our study is in agreement with the results of a study on manganese scavenging and oxidation at the Endeavour field hydrothermal vents by Mandernack and Tebo (1993). These authors registered significant particulate manganese formation in the near-field plume samples, which was attributed primarily to chemical processes, such as co-precipitation or adsorption of Mn(II) with other minerals, possibly iron oxyhydroxides.

The abundance of quartz, feldspar, illite and chlorite in the ridge flank sediments reflects predominant terrigenous input. Fe-rich montmorillonite found in both near-vent and ridge flank sediments could be attributed to its authigenic deposition, as the detrital clay mineral assemblage of the North Pacific sediments is represented by abundant illite and chlorite derived from aeolian dust (Kadko, 1985; Chamley, 1989). The most probable mechanism of formation of Fe-rich smectites, excluding pure hydrothermal nontronite, is considered to be interaction between biogenic silica and hydrothermal iron (Hein et al., 1979; Cole, 1985; Leinen, 1987). The presence of Fe-rich montmorillonite in surface sediments indicates that its formation has taken place in an oxic environment, probably at the sediment/water interface or/and within the plume. The latter suggestion is based on the fact that Dymond and Roth (1988) registered a 15–16 Å clay mineral that could be smectite of hydrothermal origin in samples containing suspended particles at Endeavour ridge. Similarly to Endeavour, it could be inferred that Fe-rich montmorillonite of Nootka is authigenic in origin.

5.2.2. *Geochemistry*

The decrease of the concentrations of Fe, Cu, Zn, Pb, As, Mo and Au in sediments away from the vents likely reflects progressive decrease of hydrothermal input with the lateral dispersal of the neutrally buoyant plume. The trend is consistent with the results of settling fluxes of plume particles at the Endeavour ridge showing that near-field particle flux exceeds that 2 km away by a factor of 10–20 and is relatively enriched in Fe, Cu and organic C (Dymond and Roth, 1988). Despite the general trend of decreasing element contents away from the vents, the individual elements show different distribution patterns, which are determined by the distribution of their carrier mineral phases. Fig. 13 demonstrates the distributions of Ba, Cu and Zn as element/Fe ratios and compares them to Cu/Fe and Zn/Fe ratios determined in a neutrally buoyant plume over the Endeavour vent fields (Feely et al., 1992). High values of Cu/Fe ratio in the near-vent sediments are comparable to that in the plume. The sharp drop of Cu/Fe ratio in sediments away from the hydrothermal venting indicates that a large part of the Cu was deposited in proximity to the vents. Similar results were obtained from studies of element distribution in the neutrally buoyant plume over the Endeavour segment (Feely et al., 1992, 1994). The authors related high enrichment in particulate Cu over the vents to presence of Cu-sulfides and interpreted the rapid decrease of Cu away from the vent field as evidence for Cu loss due to differential sedimentation, dissolution, and/or biological repackaging and sedimentation processes. Our study shows that, in addition to sulfides, Cu was deposited near the vents in Mn–Fe oxyhydroxides. Away from the vents, Cu is in Fe–Mn oxyhydroxides and in aluminosilicate phases such as Fe-rich montmorillonite.

The near-vent sediments are less enriched in Zn and Pb than in Cu, and Zn/Fe and Pb/Fe (not shown) ratios display

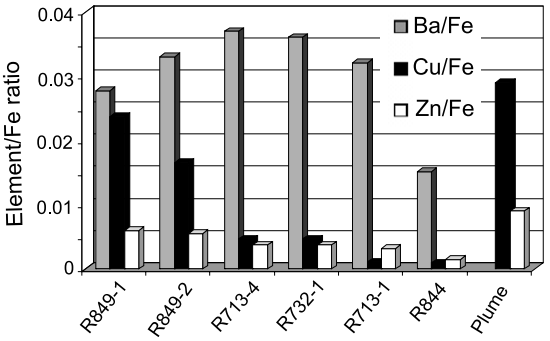

Fig. 13. Variations of element/Fe ratios in sediments with, from left to right, increasing distance from hydrothermal venting. Shown also are Cu/Fe and Zn/Fe ratios (data for Ba are not available) for a neutrally buoyant plume over Endeavour vent fields (Feely et al., 1992).

more moderate decrease away from the vent field (Fig. 13). The dominant portion of Pb and a large portion of Zn settled in both near-vent and ridge flank sediments in Fe–Mn oxyhydroxides. Ba/Fe ratios do not decrease with increasing distance from the vent field suggesting that Ba was more widely dispersed in fine-grained barite. The possibility of additional hydrothermal sources on the flanks of the Endeavour ridge affecting the geochemistry of the sediments cannot be excluded. We consider that the association of trace metals with Fe–Mn oxyhydroxides corresponds mainly to processes of scavenging of trace metals by oxyhydroxides that took place within the plume. Post-depositional oxidation of sulfides and absorption of the released components by oxyhydroxides may have additionally contributed to enrichment of oxyhydroxides in trace metals.

6. CONCLUSIONS

The studied near-vent and ridge flank sediments of the Endeavour segment, oxidized sulfides and oxyhydroxide deposits at the Main Endeavour field, as well as oxyhydroxides occurring as seafloor deposits and external chimney crusts at the Mothra field, display various geochemical, mineralogical and morphological characteristics relevant to their diverse origin.

The near-vent and ridge flank sediments are composed of variable amounts of biogenic detritus, basalt fragments, sulfides, Fe–Si ± S-rich and Mn–Fe–Si-rich phases, barite, authigenic Fe-rich montmorillonite, chlorite, illite, quartz, feldspar and calcite. The hydrothermal material in the sediments is exclusively derived from plume fallout. Sulfides are only a minor component of the near-vent sediments (approximately 2–4 wt%) and were not detected in the ridge flank sediments. We suggest that the distribution pattern of sulfides in sediments reflect mainly processes of aggregation and rapid settling from the plume and is affected to a lesser extent by pre- and post-depositional dissolution/oxidation. Characteristic feature of the near-vent sediments is the presence of aggregates of gel-like material and fine-grained particles composed of Mn–Fe–Si-rich phases containing some Ca, Mg, P, Cu and Zn. The occurrence of such phases could be a local phenomenon determined by the style of venting of the nearby structures (conductive cooling versus high-temperature mixing with seawater) and biogenic productivity.

The decrease in the concentrations of Cu, Zn, Pb, As, Mo and Au from near-vent to ridge flank sediments likely reflects dispersal and deposition of plume particulate matter with increasing distance from high-temperature venting. The abundance of Cu in the near-vent sediments and the sharp drop of Cu concentrations away from the vents are interpreted to correspond to rapid deposition of a large portion of Cu as sulfides adjacent to the vents. Part of Cu and Zn and significant portion of Pb was deposited near the vents also in Fe–Mn oxyhydroxides. In the ridge flank sediments, in addition to Fe–Mn oxyhydroxides, important carriers of trace metals are aluminosilicate phases, authigenic Fe-rich montmorillonite in particular. The REE patterns of sediments are dominated by detrital input and show variable seawater influence as illustrated by a negative Ce anomaly. The high-temperature signature of the fluids that precipitated hydrothermal material in sediments, expressed by a positive Eu anomaly, is evident only in the REE pattern of near-vent sediment.

Oxyhydroxide deposits at the Main Endeavour field are interpreted to have originated from oxidation of mound sulfides accompanied by precipitation of primary Fe-oxyhydroxide + silica from low-temperature fluids indicated by a negative Eu anomaly in the REE pattern. We suggest that oxyhydroxide deposits at Mothra originated from direct precipitation of Fe-oxyhydroxide + Mn + silica from fluids less diluted with seawater as indicated by a positive Eu anomaly. Both oxyhydroxides at the Main Endeavour field and Mothra have high trace metal contents that point to proximity to sulfide deposits. The unique microtextures of the oxyhydroxide deposits and the chimney crusts appear to have been produced by communities of diverse microorganisms inhabiting environments of diffuse venting at the Endeavour segment.

The present study demonstrates a connection between the composition of hydrothermal precipitates and the type of hydrothermal venting at the Endeavour segment, Juan de Fuca Ridge. The different pathways by which trace elements can be incorporated within various metalliferous deposits provide particular geochemical signals that can be used as an exploration guide to VMS ores. Future studies based on an expanded set of sediments and oxyhydroxide deposits from different vent fields, particularly from back-arc environments that are favored by ancient VMS ores, will be undertaken in order to understand more fully the interrelations among the various components of the hydrothermal systems.

ACKNOWLEDGMENTS

We thank co-chief scientists J. Delaney and D. Kelly, the captain and crew of R/V Thomas G. Thompson and the ROPOS crew of the expeditions in 2003 and 2004 supported by the Keck Foundation. We thank J. Gill for providing REE data for basalts from the Endeavour segment. Funding also came from the Natural Sciences and Engineering Research Council of Canada. We thank R. Haymon and an anonymous reviewer for their constructive suggestions that helped to improve the manuscript.

APPENDIX A

Bulk geochemical data

Sample	SiO_2 (wt%)	Al_2O_3 (wt%)	TiO_2 (wt%)	Fe_2O_3 (wt%)	MnO (wt%)	MgO (wt%)	CaO (wt%)	Na_2O (wt%)	K_2O (wt%)	P_2O_5 (wt%)	S (wt%)	Cr (ppm)	Co (ppm)	Ni (ppm)	Cu (ppm)
R711-3a chimney sulfide, Mothra	30.3	1.0	n.d.	17.8	0.15	0.2	0.2	0.4	0.2	n.d.	10.9	n.d.	n.d.	n.d.	130
R711-3b chimney oxyhydr., Mothra	13.4	0.6	0.01	31.2	1.01	0.6	0.7	1.5	0.3	0.5	8.8	12	n.d.	n.d.	236
R851 seafloor oxyhydr., Mothra	25.7	1.9	0.10	29.6	1.30	4.3	1.3	3.8	0.5	1.7	1.0	23	22	n.d.	1915
R710-15 sulfidic sed., Endeavour	2.3	0.3	0.02	49.0	0.04	0.7	0.1	0.8	0.1	0.2	27.4	20	223	n.d.	53,305
R714-13 ochre, Endeavour	20.1	1.5	0.10	52.3	0.19	1.6	0.6	3.4	0.4	3.0	2.5	33	58	n.d.	15,988
R714-12 ochre, Endeavour	38.7	5.0	0.35	37.2	0.43	2.9	1.2	0.8	0.9	2.5	1.1	56	47	n.d.	7749
R849-1 near-vent sed., Endeavour	36.9	6.5	0.72	25.2	1.13	4.2	3.9	2.1	0.8	1.1	2.2	83	76	49	6122
R849-2 near-vent sed., Endeavour	51.0	8.6	0.57	18.1	1.07	4.0	4.5	2.1	1.4	0.7	0.9	67	37	44	2782
Endeavour ridge flank sediments															
R713-4	44.9	8.7	0.55	10.8	1.27	3.4	11.6	1.0	1.3	0.6	0.1	54	22	75	532
R713-3	48.2	8.4	0.57	15.0	0.98	4.1	9.4	1.0	1.4	0.5	0.1	70	22	76	546
R713-2	55.3	11.6	0.77	9.2	0.64	4.3	7.0	1.2	1.8	0.3	0.1	55	22	65	145
R713-1	56.7	11.4	0.75	9.3	0.18	4.6	6.7	1.2	1.9	0.2	0.1	94	21	34	156
R732-1a (0–1 cm)	56.3	11.3	0.71	11.1	0.72	4.4	4.5	1.1	1.8	0.3	0.1	60	22	77	251
R732-1b (1–5.5 cm)	56.8	11.0	0.70	11.3	0.24	4.7	4.8	1.1	1.8	0.2	0.1	60	20	100	252
R732-1c (5.5–12 cm)	57.0	11.2	0.71	10.5	0.15	4.7	5.2	1.3	1.9	0.2	0.1	62	19	108	272
R732-1d (12–18 cm)	56.1	10.0	0.64	11.5	0.14	4.7	5.9	1.2	1.8	0.2	0.1	70	20	103	369
R732-1e (18–24 cm)	56.2	9.7	0.63	12.4	0.12	4.9	5.6	1.2	1.8	0.2	0.1	69	20	87	382
R732-2a (0–1 cm)	56.0	11.1	0.71	11.1	0.47	4.6	4.9	1.2	1.8	0.3	0.1	93	19	40	250
R732-2b (1–5.5 cm)	57.2	11.3	0.72	10.7	0.16	4.8	5.5	1.2	1.9	0.2	0.1	62	20	90	272
R732-2c (5.5–11 cm)	57.1	11.0	0.70	10.6	0.14	4.7	4.9	1.2	1.9	0.2	0.1	61	20	120	253
R732-2d (11–16 cm)	56.7	10.2	0.66	11.9	0.14	4.8	5.5	1.1	1.7	0.2	0.1	67	21	99	362
R732-2e (16–22 cm)	57.1	10.3	0.66	11.3	0.13	4.7	5.5	1.2	1.8	0.2	0.1	67	20	98	372
Nootka sediments															
R844-1a (0–2 cm)	60.0	13.2	0.79	6.5	0.11	4.2	2.5	2.5	1.8	0.2	0.3	63	12	55	52
R844-1b (2–6 cm)	61.2	13.3	0.81	6.5	0.07	4.1	2.5	2.1	1.8	0.2	0.2	64	12	70	47
R844-1c (6–11 cm)	61.7	13.5	0.82	6.6	0.06	4.1	2.5	2.5	1.9	0.2	0.3	62	11	70	56
R844-1d (11–17 cm)	61.9	13.4	0.84	6.5	0.06	4.1	2.5	2.2	1.9	0.2	0.2	65	12	44	53
R844-6	60.4	13.8	0.83	7.1	0.06	4.4	3.2	2.4	1.8	0.2	0.2	62	13	48	40

(*continued on next page*)

Appendix A (*continued*)

Sample	Pb (ppm)	Zn (ppm)	As (ppm)	Mo (ppm)	Ba (wt%)	Au (ppb)	U (ppm)	La (ppm)	Ce (ppm)	Nd (ppm)	Sm (ppm)	Eu (ppm)	Tb (ppm)	Yb (ppm)	Lu (ppm)
R711-3a chimney sulfide, Mothra	2313	4764	775	75	11.43	485	3.6	n.a.	n.a.	n.a.	n.a.	n.a.	n.a.	n.a.	n.a.
R711-3b chimney oxyhydr., Mothra	11,625	7113	577	196	13.18	154	22.9	8.94	6	9	0.48	0.50	n.d.	n.d.	n.d.
R851 seafloor oxyhydr., Mothra	761	3555	139	41	1.26	40	5.1	7.28	7	6	1.19	0.51	0.1	0.78	0.16
R710-15 sulfidic sed., Endeavour	239	15,443	119	169	0.33	28	4.0	n.d.	n.d.	n.d.	n.d.	n.d.	n.d.	n.d.	n.d.
R714-13 ochre, Endeavour	862	5520	211	123	0.72	59	30.3	14.72	14	9	2.12	1.72	0.4	1.55	0.26
R714-12 ochre, Endeavour	1230	2682	255	113	1.60	70	18.3	13.44	20	17	2.97	1.05	0.5	1.65	0.34
R849-1 near-vent sed., Endeavour	307	1590	89	42	0.73	42	3.2	15.89	22	15	3.71	1.36	0.7	2.87	0.46
R849-2 near-vent sed., Endeavour	212	1018	58	17	0.65	34	3.7	21.82	32	24	4.64	1.28	0.8	2.89	0.47
Endeavour ridge flank sediments															
R713-4	129	377	32	4	0.36	18	2.0	22.98	34	24	4.87	1.19	0.8	2.88	0.46
R713-3	138	404	36	4	0.41	21	2.4	24.98	32	26	5.22	1.30	0.8	3.30	0.53
R713-2	44	253	6	1	0.30	17	3.2	23.45	44	27	4.94	1.15	0.7	2.58	0.41
R713-1	43	276	6	1	0.31	17	4.8	24.21	49	27	5.10	1.20	0.8	2.84	0.46
R732-1a (0–1 cm)	74	354	10	2	0.36	20	6.1	23.84	43	25	5.19	1.20	0.8	2.69	0.44
R732-1b (1–5.5 cm)	70	353	7	1	0.35	22	6.2	24.19	44	25	5.35	1.21	0.8	2.71	0.43
R732-1c (5.5–12 cm)	67	357	3	1	0.36	22	6.1	24.67	40	26	5.38	1.24	0.8	3.06	0.47
R732-1d (12–18 cm)	66	342	5	1	0.34	22	6.8	24.00	38	25	5.18	1.32	0.8	3.12	0.51
R732-1e (18–24 cm)	75	346	6	1	0.33	22	6.4	23.51	37	25	5.02	1.21	0.8	3.10	0.48
R732-2a (0–1 cm)	74	344	5	1	0.35	19	2.3	24.18	48	27	5.16	1.29	0.8	2.81	0.44
R732-2b (1–5.5 cm)	75	396	4	1	0.36	19	4.1	24.23	43	27	5.10	1.23	0.7	2.90	0.46
R732-2c (5.5–11 cm)	76	352	3	1	0.35	19	4.2	24.50	42	27	5.10	1.23	0.8	2.90	0.50
R732-2d (11–16 cm)	63	335	6	1	0.35	23	6.7	24.70	39	27	5.31	1.38	0.9	3.11	0.50
R732-2e (16–22 cm)	77	355	6	1	0.34	21	6.6	24.44	39	27	5.36	1.37	0.9	3.15	0.49
Nootka sediments															
R844-1a (0–2 cm)	n.d.	92	3	1	0.10	7	4.7	17.88	38	20	3.82	1.02	0.6	1.96	0.32
R844-1b (2–6 cm)	n.d.	91	2	1	0.10	6	2.8	17.38	37	20	3.79	0.98	0.5	1.92	0.31
R844-1c (6–11 cm)	n.d.	101	3	2	0.10	7	2.1	17.85	38	20	3.91	1.01	0.5	2.10	0.32
R844-1d (11–17 cm)	n.d.	102	2	2	0.10	7	3.8	18.12	39	21	3.94	0.98	0.6	2.06	0.33
R844-6	n.d.	75	3	2	0.07	6	1.8	17.74	39	20	3.99	1.06	0.6	2.18	0.32

n.d., not determined; n.a., not analysed.

REFERENCES

Aoki S., Kohyama N., and Sudo T. (1974) An iron-rich montmorillonite in a sediment core from the northeastern Pacific. *Deep Sea Res.* **21**, 865–875.

Aoki S., Kohyama N., and Sudo T. (1979) Mineralogical and chemical properties of smectites in a sediment core from the southeastern Pacific. *Deep Sea Res.* **26A**, 893–902.

Baker E. T., and Massoth G. J. (1987) Characterization of hydrothermal plumes from two vent fields on the Juan de Fuca Ridge, northeast Pacific Ocean. *Earth Planet. Sci. Lett.* **85**, 59–73.

Barnes S., and Gorton M. P. (1984) Trace element analysis by neutron activation with a low flux reactor (Slowpoke-II), results for international reference rocks. *Geostandard. Newslett.* **8**, 17–23.

Barrett T. J., Taylor P. N., and Lugowski J. (1987) Metalliferous sediments from DSDT Leg 92: the East Pacific Rise transect. *Geochim. Cosmochim. Acta* **51**, 2241–2253.

Bennett J. C., and Tributsch H. (1978) Bacterial leaching patterns on pyrite crystal surface. *J. Bacteriol.* **134**, 310–317.

Benjamin S. B., and Haymon R. M. (2006) Hydrothermal mineral deposits and fossil biota from a young (0.1 Ma) abyssal hill on the flank of the fast spreading East Pacific Rise: evidence for pulsed hydrothermal flow and tectonic tapping of axial heat and fluids. *Geochem. Geophys. Geosys.* **7**, Q05002. doi:10.1029/2005GC001011.

Binns R. A., Scott S. D., Bogdanov Y. A., Lisitzin A. P., Gordeev V. V., Gurvich E. G., Finlayson E. J., Boyd T., Dotter L. E., Wheller G. E., and Muravyev K. G. (1993) Hydrothermal oxide and gold-rich sulfate deposits of Franklin Seamount, western Woodlark Basin, Papua New Guinea. *Econ. Geol.* **88**, 2122–2153.

Biscaye P. E. (1965) Mineralogy and sedimentation of recent deep-sea clay in the Atlantic Ocean and adjacent seas and oceans. *Geol. Soc. Am. Bull.* **76**, 803–832.

Boström K., and Peterson M. N. A. (1969) The origin of aluminum-poor ferromanganoan sediments of high heat flow on the East Pacific Rise. *Mar. Geol.* **7**, 427–447.

Boyd T., and Scott S. D. (1999) Two-XRD-line ferrihydrite and Fe–Si–Mn oxyhydroxide mineralization from Franklin Seamount, western Woodlark Basin, Papua New Guinea. *Can. Miner.* **37**, 973–990.

Boyd T., and Scott S. D. (2001) Microbial and hydrothermal aspects of ferric oxyhydroxides and ferrosic hydroxides: the example of Franklin Seamount, Western Woodlark Basin, Papua New Guinea. *Geochem. Trans.* **7**. doi:10.1039/b105277m.

Boyd T., Scott S. D., and Hekinian R. (1993) Trace element patterns in Fe–Si–Mn oxyhydroxides at three hydrothermally active seafloor regions. *Res. Geol.* **17**, 83–95, Spec. Issue.

Butterfield D. A., McDuff R. E., Mottl M. J., Lilley M. D., Lupton J. E., and Massoth G. J. (1994) Gradients in the composition of hydrothermal fluids from the Endeavour segment vent field: phase separation and brine loss. *J. Geophys. Res.* **99**(B5), 9561–9583.

Chamley H. (1989) *Clay Sedimentology*. Springer-Verlag, Berlin, Heidelberg.

Chavagnac V., German Ch. R., Milton J. A., and Palmer M. R. (2005) Sources of REE in sediment cores from the Rainbow vent site (36°14′N, MAR). *Chem. Geol.* **216**, 329–352.

Cole T. G. (1985) Composition, oxygen isotope geochemistry, and origin of smectite in the metalliferous sediments of the Bauer Deep, southeast Pacific. *Geochim. Cosmochim. Acta* **49**, 221–235.

De Baar H. J. W., Bacon M. P., Brewer P. G., and Bruland K. W. (1985) Rare earth elements in the Pacific and Atlantic Oceans. *Geochim. Cosmochim. Acta* **49**, 1943–1959.

Delaney J. R., McDuff R. E., and Lupton J. E. (1984) Hydrothermal fluid temperatures of 400 °C on the Endeavour segment, northern Juan de Fuca. *Eos Trans. AGU* **61**, 992.

Delaney J. R., Robigou V., McDuff R. E., and Tivey M. K. (1992) Geology of a vigorous hydrothermal system on the Endeavour Segment, Juan de Fuca Ridge. *J. Geophys. Res.* **97**(B13), 19,663–19,682.

Dymond J., and Roth S. (1988) Plume dispersed hydrothermal particles: a time-series record of settling flux from the Endeavour Ridge using moored sensors. *Geochim. Cosmochim. Acta* **52**, 2525–2536.

Edwards J. K., McCollom T. M., Konishi H., and Buseck P. R. (2003) Seafloor bioalteration of sulfide minerals: results from in situ incubation studies. *Geochim. Cosmochim. Acta* **67**, 2843–2856.

Feely R. A., Lewison M., Massoth G. J., Robert-Baldo G., Lavelle W., Byrne R. H., von Damm K. V., and Curl, Jr., H. C. (1987) Composition and dissolution of black smoker particles from active vents on the Juan de Fuca Ridge. *J. Geophys. Res.* **92**(B11), 11,347–11,363.

Feely R. A., Massoth G. J., Baker E. T., Lebon T. G., and Geiselman T. L. (1992) Tracking the dispersal of hydrothermal plumes from the Juan de Fuca Ridge using suspended matter composition. *J. Geophys. Res.* **97**, 3457–3468.

Feely R. A., Massoth G. J., Trefry J. H., Baker E. T., Paulson A. J., and Lebon G. T. (1994) Composition and sedimentation of hydrothermal plume particles from North Cleft segment, Juan de Fuca Ridge. *J. Geophys. Res.* **99**, 4985–5006.

German C. R., Bourlès D. L., Brown E. T., Hergt J., Colley S., Higgs N. C., Ludford E. M., Nelsen T. A., Feely R. A., Raisbeck G., and Yiou F. (1997) Hydrothermal scavenging on the Juan de Fuca Ridge: $^{230}Th_{xs}$, ^{10}Be, and REEs in ridge-flank sediments. *Geochim. Cosmochim. Acta* **61**, 4067–4078.

German C. R., Hergt J., Palmer M. R., and Edmond J. M. (1999) Geochemistry of a hydrothermal sediment core from the OBS vent-field, 21°N East Pacific Rise. *Chem. Geol.* **155**, 65–75.

German C. R., Higgs N. C., Thomson J., Mills R., Elderfield H., Blusztajn J., Fleer A. P., and Bacon M. P. (1993) A geochemical study of metalliferous sediment from the TAG hydrothermal mound, 26°08′N, Mid-Atlantic Ridge. *J. Geophys. Res.* **98**, 9683–9692.

German C. R., Klinkhammer G. P., Edmond J. M., Mitra A., and Elderfield H. (1990) Hydrothermal scavenging of rare earth elements in the ocean. *Nature* **345**, 516–518.

Goodfellow W. D., and Peter J. M. (1994) Geochemistry of hydrothermally altered sediment, Middle Valley, northern Juan de Fuca Ridge. Sites 855–858 Middle Valley, Juan de Fuca Ridge. In *Proc. ODP, Sci. Results*, vol. 139 (eds. N. K. McQuistion and L. H. Dearmont). pp. 207–291.

Güven N. (1988) Smectites. In *Hydrous Phyllosilicates (Exclusive of Micas)* (ed. S. W. Baley). Rev. Mineral. **19**, Min. Soc. Am., pp. 497–552.

Hannington M. D., Thompson G., Rona P. A., and Scott S. D. (1988) Gold and native copper in supergene sulphides from the Mid-Atlantic Ridge. *Nature* **333**, 64–66.

Haymon R. M., and Kastner M. (1981) Hot spring deposits on the East Pacific Rise at 21°N: preliminary description on mineralogy and genesis. *Earth Planet. Sci. Lett.* **53**, 363–381.

Hein J. R., Koschinsky A., Bau M., and Manheim F.T. (1999) Cobalt-rich ferromanganese crusts in the Pacific. In *Handbook of Mineral Deposits* (ed. D. Cronan) CRC Marine Science Series, pp. 239–280.

Hein J. R., Yeh H.-W., and Alexander E. (1979) Origin of iron-rich montmorillonite from the manganese nodule belt of the north equatorial Pacific. *Clay. Clay. Miner.* **27**, 185–194.

Hekinian R., Hoffert M., Larqué P. h., Cheminée J. L., Stoffers P., and Bideau D. (1993) Hydrothermal Fe and Si oxyhydroxide deposits from South Pacific intraplate volcanoes and East Pacific Rise axial and off axis regions. *Econ. Geol.* **88**, 2099–2121.

Herzig P. M., Hannington M. D., Scott S. D., Maliotis G., Rona P. A., and Thompson G. (1991) Gold-rich seafloor gossans in the Troodos ophiolite and on the Mid-Atlantic Ridge. *Econ. Geol.* **86**, 1747–1755.

Juniper S. K., and Fouquet Y. (1988) Filamentous iron-silica deposits from modern and ancient hydrothermal sites. *Can. Miner.* **26**, 859–869.

Kadko D. (1985) Late Cenozoic sedimentation and metal deposition in the North Pacific. *Geochim. Cosmochim. Acta* **49**, 651–661.

Kadko D. C., Rosenberg N. D., Lupton J. E., Collier R. W., and Lilley M. D. (1990) Chemical reaction rates and entrainment within the Endeavour Ridge hydrothermal plume. *Earth Planet. Sci. Lett.* **99**, 315–335.

Kalogeropoulos S. I., and Scott S. D. (1983) Mineralogy and geochemistry of tuffaceous exhalites (tetsusekiei) of the Fukazawa mine, Hokuroku district, Japan. *Econ. Geol. Monogr.* **5**, 412–432.

Kalogeropoulos S. I., and Scott S. D. (1989) Mineralogy and geochemistry of an Archean tuffaceous exhalite, the Main Contact Tuff, Millenbach mine area, Noranda, Quebec. *Can. J. Earth Sci.* **26**, 88–105.

Karsten J. L., Hammond S. R., Davis E. E., and Currie R. G. (1986) Detailed geomorphology and neotectonics of the Endeavour Segment, Juan de Fuca Ridge: New results from Seabeam swath mapping. *Geol. Soc. Am. Bull.* **95**, 930–945.

Kelley D. S., Delaney J. R., Lilley M. D., and Butterfield D. A. (2001a) Vent field distribution and evolution along the Endeavour Segment, Juan de Fuca Ridge. *Eos Trans. AGU*, **82** (47), Fall Meet. Suppl., Abstract OS21B-0439.

Kelley D. S., Delaney J. R., and Yorger D. R. (2001b) Geology and venting characteristics of the Mothra hydrothermal field, Endeavour segment, Juan de Fuca Ridge. *Geology* **29**, 959–962.

Kennedy C. B., Scott S. D., and Ferris F. G. (2003) Characterization of bacteriogenic iron oxide deposits from Axial Volcano, Juan de Fuca Ridge, north-east Pacific Ocean. *Geomicrobiol. J.* **20**, 199–214.

Klinkhammer G. P., Elderfield H., Edmond J. M., and Mitra A. (1994) Geochemical implications of rare earth element patterns in hydrothermal fluids from mid-ocean ridges. *Geochim. Cosmochim. Acta* **58**, 5105–5113.

Kristall B., Kelley D. S., Hannington M. D., and Delaney J. R. (2006) Growth history of a diffusely venting sulfide structure from the Juan de Fuca Ridge: a petrological and geochemical study. *Geochem. Geophys. Geosys.* **7**, Q07001. doi:10.1029/2005GC001166.

Kyte F. T., Leinen M., Heath G. R., and Zhou L. (1993) Cenozoic sedimentation history of the central North Pacific: Inferences from the element geochemistry of core LL44-GPC3. *Geochim. Cosmochim. Acta* **57**, 1719–1740.

Leinen M. (1987) The origin of paleochemical signatures in North Pacific pelagic clays: Partitioning experiments. *Geochim. Cosmochim. Acta* **51**, 305–319.

Lupton J. E., Delaney J. E., Johnson H. P., and Tivey M. K. (1985) Entrainment and vertical transport of deep-ocean water by buoyant hydrothermal plumes. *Nature* **316**, 621–623.

Mandernack K. W., and Tebo B. M. (1993) Manganese scavenging and oxidation at hydrothermal vents and in vent plumes. *Geochim. Cosmochim. Acta* **57**, 3907–3923.

Michard A., Michard G., Stüben D., Stoffers P., Cheminée J.-L., and Binard N. (1993) Submarine thermal springs associated with young volcanoes: the Teahitia vents, Society Islands, Pacific Ocean. *Geochim. Cosmochim. Acta* **57**, 4977–4986.

Mills R. A. (1995) Hydrothermal deposits and metalliferous sediments from TAG, 26°N Mid-Atlantic Ridge. In *Hydrothermal Vents and Processes* (eds. L. M. Parson, C. L. Walker and D. R. Dixon). Geological Society Special Publication No. 87, pp. 121–132.

Mills R. A., and Elderfield H. (1995) Rare earth element geochemistry of hydrothermal deposits from the active TAG Mound, 26°N Mid-Atlantic Ridge. *Geochim. Cosmochim. Acta* **59**, 3511–3524.

Mills R., Elderfield H., and Thomson J. (1993) Dual origin for the hydrothermal component in a metalliferous sediment core from the Mid-Atlantic Ridge. *J. Geophys. Res.* **98**, 9671–9681.

Mills R. A., Thomson J., Elderfield H., Hinton R. W., and Hyslop E. (1994) Uranium enrichment in metalliferous sediments from the Mid-Atlantic Ridge. *Earth Planet. Sci. Lett.* **124**, 35–47.

McConachy T. F., and Scott S. D. (1987) Real-time mapping of hydrothermal plumes over southern Explorer Ridge, NE Pacific Ocean. *Mar. Mining* **6**, 181–204.

Mustin C., Berthelin J., Marion P., and de Donato P. (1992) Corrosion and electrochemical oxidation of pyrite by *Thiobacillus ferrooxidans*. *Appl. Environ. Microbiol.* **58**, 1175–1182.

Peter J. M., and Goodfellow W. D. (1996) Mineralogy, bulk and rare earth element geochemistry of massive sulphide-associated hydrothermal sediments of the Brunswick Horizon, Bathurst mining camp, New Brunswick. *Can. J. Earth Sci.* **33**, 252–283.

Peter J. M., Kjarsgaard I. M., and Goodfellow W. D. (2003) Hydrothermal sedimentary rocks of the Heath Steele Belt, Bathurst Mining Camp, New Brunswick: part 1. Mineralogy and mineral chemistry. *Econ. Geol. Monogr.* **11**, 361–390.

Piper D. Z. (1974) Rare earth elements in ferromanganese nodules and other marine phases. *Geochim. Cosmochim. Acta* **38**, 1007–1022.

Puteanus D., Glasby G. P., Stoffers P., and Kunzendorf H. (1991) Hydrothermal iron-rich deposits from the Teahitia-Mehitia and Macdonald hot spot areas, Southwest Pacific. *Mar. Geol.* **98**, 389–409.

Rona P. A., Bemis K. G., Jackson D. R., Jones C. D., Mitsuzawa K., Palmer D. R., and Silver D. (2002) Effect of tidal cycle on entrainment by the Grotto vent plume, Main Endeavour Field, Juan de Fuca Ridge. *Eos Trans. AGU*, **83** (47), Fall Meet. Suppl., Abstract OS52D-0254.

Ruhlin D. E., and Owen R. M. (1986) The rare earth element geochemistry of hydrothermal sediments from the East Pacific Rise; examination of a seawater scavenging mechanism. *Geochim. Cosmochim. Acta* **50**(3), 393–400.

Scott S. D. (1997) Seafloor hydrothermal systems and deposits. In *Geochemistry of Hydrothermal Ore Deposits*, 3rd ed. (ed. H. L. Barnes). John Wiley and Sons, New York, pp. 797–875.

Scholten J. C., Scott S. D., Garbe-Schönberg D., Fietzke J., Blanz T., and Kennedy C.B. (2004) Hydrothermal iron and manganese crusts from the Pitcairn hotspot region. In *Oceanic Hotspots. Intraplate Submarine Magmatism and Tectonism* (ed. R. Hekinian). Springer-Verlag, pp. 375–405.

Stix J., and Gorton M. P. (1992) Trace element analysis of ten U.S. Geological Survey rock standards by neutron activation using a low flux reactor. *Geostandard. Newslett.* **16**, 21–26.

Straube W. L., Deming J. W., Somervile C. C., Colwell R. R., and Baross J. A. (1990) Particulate DNA in smoker fluids: evidence for existence of microbial populations in hot hydrothermal systems. *Appl. Environ. Microbiol.* **56**, 1440–1447.

Thomson R. E., Delaney J. R., McDuff R. E., Janecky D. R., and McClain J. S. (1992) Physical characteristics of the Endeavour

Ridge hydrothermal plume during July 1988. *Earth Planet. Sci. Lett.* **111**, 141–154.

Thomson R. E., Mihály S. F., Rabinovich A. B., McDuff R. E., Veirs S. R., and Stahr F. R. (2003) Constrained circulation at Endeavour ridge facilitates colonization by vent larvae. *Nature* **424**, 545–549.

Tivey M. K., and Delaney J. R. (1985) Controls on the distribution and size of hydrothermal vent structures on the Endeavour Segment, Juan de Fuca Ridge. *Eos Trans. AGU* **66**, 926.

Tivey M. K., and Delaney J. R. (1986) Growth of large sulfide structures on the Endeavour Segment of the Juan de Fuca Ridge. *Earth Planet. Sci. Lett.* **77**, 303–317.

Tivey M. A., and Johnson H. P. (1987) The central anomaly magnetic high: implications for ocean crust construction and evolution. *J. Geophys. Res.* **92**, 12,685–12,694.

Tivey M. K., Stakes D. S., Cook T. L., Hannington M. D., and Peterson S. (1999) A model for growth of steep-sided vent structures on the Endeavour Segment of the Juan de Fuca Ridge: results of a petrologic and geochemical study. *J. Geophys. Res.* **104**, 22,859–22,883.

Toyoda K., and Masuda A. (1991) Chemical leaching of pelagic sediments: identification of the carriers of Ce anomaly. *Geochem. J.* **25**, 95–119.

Verati C. h., de Donato P., Prieur D., and Lancelot J. (1999) Evidence of bacterial activity from micrometer-scale layer analyses of black-smoker sulfide structures (Pito Seamount site, Easter microplate). *Chem. Geol.* **158**, 257–269.

Associate editor: Frank A. Podosek